© 2017. Published by The Company of Biologists Ltd | Development (2017) 144, 1841-1850 doi:10.1242/dev.144782

RESEARCH ARTICLE

Dose-dependent transduction of Hedgehog relies on phosphorylation-based feedback between the G-protein-coupled receptor Smoothened and the kinase Fused

Matthieu Sanial[1,§], Isabelle Bécam[1,§], Line Hofmann[1,*], Julien Behague[1,‡], Camilla Argüelles[1], Vanessa Gourhand[1], Lucia Bruzzone[1], Robert A. Holmgren[2] and Anne Plessis[1,¶]

ABSTRACT

Smoothened (SMO) is a G-protein-coupled receptor-related protein required for the transduction of Hedgehog (HH). The HH gradient leads to graded phosphorylation of SMO, mainly by the PKA and CKI kinases. How thresholds in HH morphogen regulate SMO to promote switch-like transcriptional responses is a central unsolved issue. Using the wing imaginal disc model in *Drosophila*, we identified new SMO phosphosites that enhance the effects of the PKA/CKI kinases on SMO accumulation, its localization at the plasma membrane and its activity. Surprisingly, phosphorylation at these sites is induced by the kinase Fused (FU), a known downstream effector of SMO. In turn, activation of SMO induces FU to act on its downstream targets. Overall, our data provide evidence for a SMO/FU positive regulatory loop nested within a multikinase phosphorylation cascade. We propose that this complex interplay amplifies signaling above a threshold that allows high HH signaling.

KEY WORDS: *Drosophila*, Signal transduction, Hedgehog, Smoothened, Phosphorylation, Fused kinase, SNAP-tag labeling

INTRODUCTION

The Hedgehog (HH) signaling pathway is crucial for the growth and patterning of many metazoans (Lee et al., 2016). Its deregulation leads to developmental disorders and cancers (Pak and Segal, 2016). In many cases, HH acts as a morphogen; it spreads as a gradient across a field of receiving cells to promote dose-dependent discrete transcriptional responses (Vervoort, 2000).

HH signaling requires Smoothened (SMO), a member of the G-protein-coupled receptor family (Ayers and Therond, 2010). SMO is regulated by the transmembrane protein Patched (PTC; Nakano et al., 1989), which acts as both an SMO antagonist and an HH co-receptor. Studies in flies show that in the absence of signal, PTC promotes SMO internalization and targeting to the lysosome for degradation (Fan et al., 2013; Li et al., 2012; Xia et al., 2012). These effects are blocked by HH, leading to accumulation of a hyperphosphorylated form of SMO at the plasma membrane. An important contribution to SMO hyperphosphorylation is the sequential action of the cAMP-dependent protein kinase (PKA) and Casein kinase 1 (CKI) on three clusters of serines (S) and threonines (T) located in its C-terminal cytoplasmic tail (cyto-tail; Chen and Jiang, 2013). These phosphorylations are necessary and sufficient for SMO localization to the plasma membrane and activation. They induce SMO clustering and a conformational switch in its cyto-tail. The extent of phosphorylation of the PKA/CKI clusters depends on HH levels and controls in a graded manner SMO clustering, the degree of conformational change in its cyto-tail, its accumulation at the cell surface and its signaling activity (Fan et al., 2012; Su et al., 2011; Zhao et al., 2007). Moreover, CKIγ/Gilgamesh (Gish), G-protein-coupled receptor kinase 2 (GPRK2/GRK2), Casein kinase II and atypical protein kinase C increase the ability of SMO to transduce high levels of HH by phosphorylating residues present in the membrane-proximal and central regions of the SMO cyto-tail (Jia et al., 2010; Jiang et al., 2014; Li et al., 2016; Maier et al., 2014). In vertebrates, SMO phosphorylation has been reported to depend on GRK2 and CKIγ (Chen et al., 2004). However, the role of GRPK2/GRK2 has recently been called into question by a study in zebrafish (Zhao et al., 2016).

The wing imaginal disc has been instrumental in study of the morphogenetic effects of HH. In this epithelium, HH is produced in the posterior (P) compartment and spreads towards the anterior (A) region. The dose of HH controls the fate of Cubitus interruptus (CI), a zinc finger transcription factor of the GLI family (Aza and Kornberg, 1999; Wang and Holmgren, 2000). In the absence of HH, CI undergoes partial degradation that leads to a truncated repressor form (CI-R). Toward the A/P boundary, the progressive suppression of CI processing by increased doses of HH leads to the gradual decrease of CI-R associated with a progressive accumulation of full-length CI (CI-FL). Thus, in the presence of low levels of HH, CI processing is blocked, which promotes *decapentaplegic* (*dpp*) expression. In the presence of intermediate levels of HH, the levels of CI-FL are increased, leading to *ptc* and *collier* (*col*; *knot*) expression. Finally, in the A cells that abut the P compartment HH producing cells, CI-FL is turned into a hyperactive state (CI-A), which enables *engrailed* (*en*) expression.

How is the graded phosphorylation of SMO transduced to the intracellular components of the pathway that regulate CI fate? In the fly wing imaginal disc, responses to high levels of HH rely on the protein kinase Fused (FU) and the kinesin Costal2 (COS2; Alves et al., 1998; Ho et al., 2005; Ohlmeyer and Kalderon, 1998). Both proteins are part of a SMO-bound large cytoplasmic complex that controls CI-FL processing, nuclear entry and activation (Jia et al., 2003; Monnier et al., 1998, 2002; Ogden et al., 2003). The relationships between SMO, FU and COS2 are very complex. SMO

[1]Institut Jacques Monod, CNRS, UMR 7592, Université Paris Diderot, Sorbonne Paris Cité, Paris F-75205, France. [2]Department of Molecular Bioscience, Northwestern University, Evanston, IL 60208-3500, USA.
*Present address: Department of Developmental and Cell Biology, University of California Irvine, Irvine, CA 92697, USA. ‡Present address: Institut Curie, Paris 75005, France.
§These authors contributed equally to this work

¶Author for correspondence (anne.plessis@ijm.fr)

A.P., 0000-0001-9193-7031

Received 21 September 2016; Accepted 20 March 2017

Development (2017) 144, 1841-1850 doi:10.1242/dev.144782

directly recruits FU to the plasma membrane and promotes its clustering and its trans-autophosphorylation, with each event being sufficient to promote FU activation (Claret et al., 2007; Shi et al., 2011). COS2 and FU control each other's levels and activity (Ruel et al., 2007; Zhou and Kalderon, 2010, 2011) and also feed back on SMO (Claret et al., 2007; Liu et al., 2007; Ranieri et al., 2014). Thus, in the absence of HH, COS2 binding to SMO inhibits its phosphorylation by PKA/CKI and its accumulation at the cell surface, whereas in response to HH, FU activity is essential for the accumulation of SMO at the plasma membrane and full phosphorylation. It has been proposed that positive feedback by FU on SMO could be attributable to FU opposing the negative effect of COS2. However, FU could control the fate of SMO by directly promoting its phosphorylation on new sites.

Here, we report the identification of four new clusters of S/T in the most C-terminal part of the SMO cyto-tail, near to where FU binds. These sites are required for the full hyperphosphorylation of SMO in response to HH. Their phosphorylation depends on SMO binding to FU and on FU kinase activity, arguing that FU might directly phosphorylate SMO. By preventing or mimicking their phosphorylation, we show that they enhance the effects of the phosphorylation of SMO by the PKA/CKI, resulting in high levels of HH signaling. Finally, phosphorylation of these sites is important for FU to phosphorylate its targets COS2 and SU(FU) and to promote high CI-FL activation. We propose that in response to high levels of HH signal, SMO and FU engage in a complex positive feedback loop, in which they mutually enhance each other's activation. This multikinase phosphorylation cascade would result in an amplification of HH signaling that reaches a threshold, promoting 'high HH'-specific responses.

RESULTS

Phosphorylation at sites near the C-terminal of SMO is required for HH-induced hyperphosphorylation

PKA and CKI act on three clusters of S/T (Fig. 1A). Blocking the phosphorylation of these residues [by replacing the PKA sites by alanines (A), $SMO^{PKA\text{-}SA}$] did not totally prevent SMO phosphorylation in response to HH (Fig. 1B). Four C-terminal (Ct) blocks (GI-GIV) of S or T residues located between amino acid (aa) 916 and 1036 are conserved among *Drosophila* species (Fig. 1A). To assay their phosphorylation, we transiently expressed wild-type SMO (SMO^{wt}) or $SMO^{Ct\text{-}SA}$ (all the Ct-sites replaced by A) – both HA tagged – in HH responsive Cl8 cells (Fig. 1B). In the presence of HH, $SMO^{Ct\text{-}SA}$-HA phosphorylation levels were significantly reduced compared with that of SMO^{wt}-HA. Mutation of both the PKA/CKI and the Ct-sites ($SMO^{PKA\text{-}SA\ Ct\text{-}SA}$-HA) almost totally suppressed SMO phosphorylation.

We conclude that, in these conditions, the Ct and PKA/CKI sites are the major contributors to the HH-induced SMO hyperphosphorylation.

Activated FU promotes the phosphorylation of the SMO Ct-sites

Downregulation of FU kinase activity reduces the hyperphosphorylation of SMO induced by HH (Liu et al., 2007), and FU is able to induce SMO phosphorylation (Claret et al., 2007). This latter effect depends on FU kinase activity and is enhanced with GAP-gFU, a constitutively active form of FU. GAP-gFU also induces the phosphorylation of $SMO^{PKA\text{-}SA}$-HA (Fig. 1C; Fig. S1A), showing that its target sites are outside the known PKA/CKI targets. The Ct clusters are at or near the FU binding region (59 most C-terminal aa) and, as shown in Fig. 1C,D, GAP-gFU could not induce $SMO^{Ct\text{-}SA}$-HA (or $SMO^{PKA\text{-}SA\ Ct\text{-}SA}$) phosphorylation, indicating that the Ct-sites are targeted by activated FU. Note that mutation of each Ct group separately impacted the SMO phosphorylation induced by GAP-cFU to various degrees (Fig. S1B), indicating that they all contribute to it.

Moreover, GAP-gFU^{DANA}, a kinase-dead form of GAP-gFU, which acts in a dominant negative manner (Claret et al., 2007), reduces the HH-induced phosphorylation of $SMO^{PKA\text{-}SD}$, but not of $SMO^{PKA\text{-}SD\ Ct\text{-}SA}$ (Fig. 1E). Finally, induction of SMO^{wt} phosphorylation by GAP-gFU was suppressed with a form of SMO lacking its FU binding region ($SMO^{\Delta 978}$-HA; Fig. S1C).

These data argue that activated FU can promote the phosphorylation of the Ct-sites involved in the HH-induced hyperphosphorylation of SMO and show that this effect is FU kinase activity and interaction dependent.

Phosphorylation of the PKA/CKI sites favors the phosphorylation of the Ct clusters

We next studied whether the phosphorylation of the PKA/CKI and Ct clusters influenced each other. As shown above, phosphorylation of the PKA sites is not required for that of the Ct-sites induced by GAP-gFU. We also tested $SMO^{PKA\text{-}SD}$-HA, in which the PKA and CKI phosphorylation sites have been replaced by aspartic acids (D) to mimic their phosphorylation. $SMO^{PKA\text{-}SD}$-HA was constitutively phosphorylated in the absence of HH (Fig. 1F; Fig. S1A), probably attributable to the phosphorylation of the Ct clusters as it disappeared with $SMO^{PKA\text{-}SD\ Ct\text{-}SA}$-HA. By contrast, $SMO^{Ct\text{-}SD}$-HA (Ct-sites replaced by D to mimick their phosphorylation) displayed no sign of phosphorylation in the absence of HH but was further phosphorylated in the presence of HH, probably on its PKA sites as this was not the case for $SMO^{PKA\text{-}SA\ Ct\text{-}SD}$-HA (Fig. S1D,E).

Finally, we analyzed the effect of Ct-sites on SMO phosphorylation *in vivo*. The *smo* transgenes (smo^{wt}, $smo^{Ct\text{-}SA}$ and $smo^{Ct\text{-}SD}$) were inserted at the same locus to ensure comparable expression levels and expressed throughout the wing primodium. As seen in Fig. 1G, blocking the phosphorylation of the Ct-sites ($smo^{Ct\text{-}SA}$) reduced the levels of SMO phosphorylation, whereas mimicking it ($smo^{Ct\text{-}SD}$) led to their increase.

In summary, the phosphorylation of the Ct-sites of SMO is neither necessary for the phosphorylation of the PKA/CKI sites in response to HH nor sufficient to promote it in the absence of HH. By contrast, phosphorylation of the PKA/CKI sites favors the phosphorylation of the Ct-sites, but is not required for their phosphorylation by activated GAP-FU, suggesting that it acts by activating FU.

Phosphorylation of the Ct-sites controls the levels of SMO

Our data indicate that the phosphorylation of the Ct-sites upregulates SMO levels (Fig. 1; Fig. S1). To quantify this, we fused SMO N-terminal to an enzymatic self-labeling tag called SNAP that enables direct detection and quantification of the tagged protein after electrophoresis (Tirat et al., 2006). After checking the functionality of SNAP-SMO *in vivo* (Fig. S2), we analyzed the effects of HH and the Ct-sites on its levels in Cl8 cells. As shown in Fig. 2A-C (and Fig. S3), HH promoted a more than twofold increase in SNAP-SMO levels. SNAP-$SMO^{Ct\text{-}SA}$ basal levels were not affected, but its HH-induced accumulation was reduced by ∼30%. Conversely, SNAP-$SMO^{Ct\text{-}SD}$) basal levels were significantly upregulated (by threefold), an effect strongly increased (sevenfold compared with SNAP-SMO^{wt}) in response to HH. Moreover, compared with SNAP-$SMO^{PKA\text{-}SD}$, SNAP-$SMO^{PKA\text{-}SD\ Ct\text{-}SA}$ levels were downregulated by about twofold both in the presence and in

Development (2017) 144, 1841-1850 doi:10.1242/dev.144782

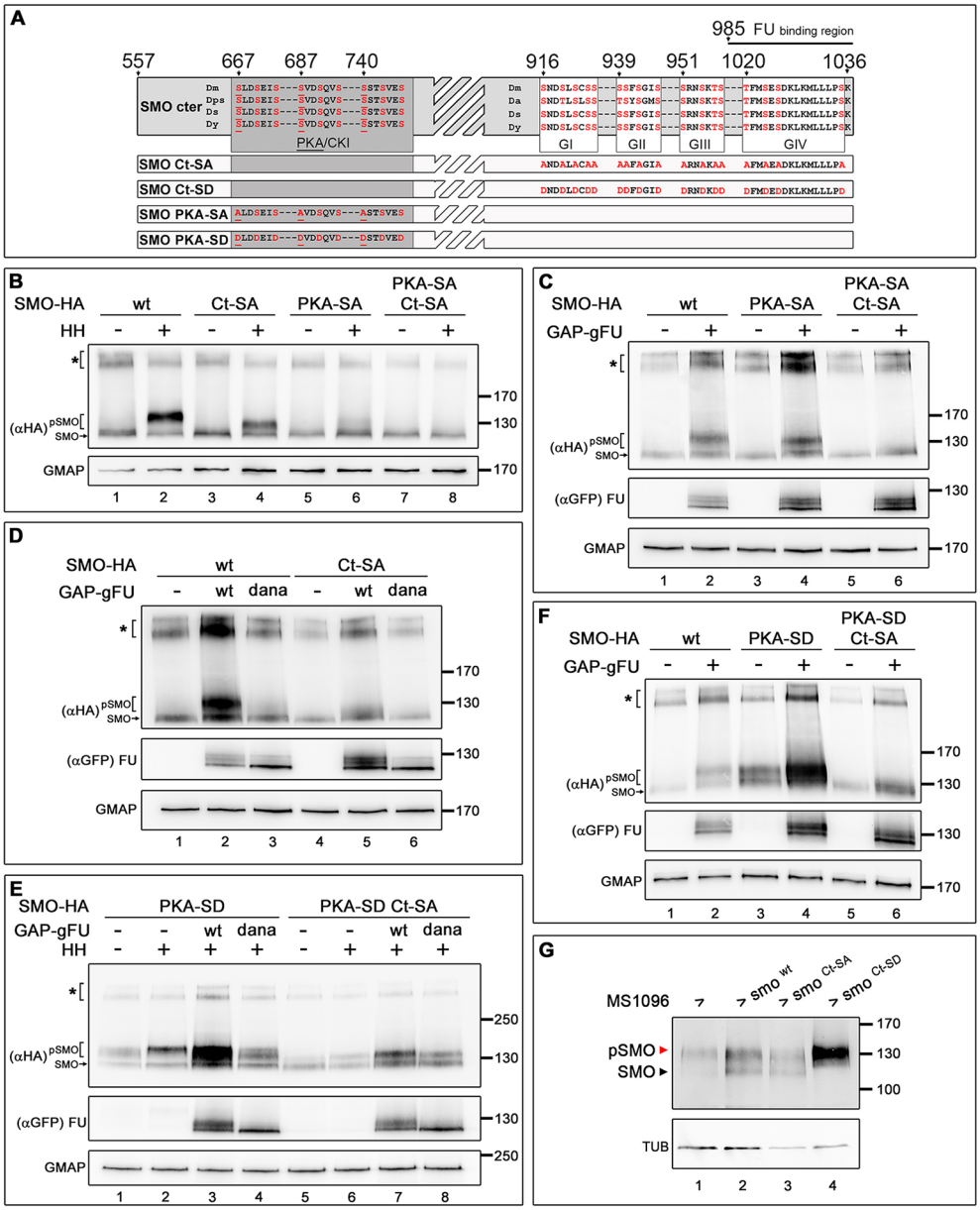

Fig. 1. Activated FU promotes the phosphorylation of SMO on new sites in its C-terminal intracellular tail. (A) Schematic representation of the *Drosophila melanogaster* SMO C-terminal from position 557 to 1036. A multiple sequence alignment of different *Drosophilae* species (Dm, *D. melanogaster*; Dps, *D. pseudoobscura*; Ds, *D. simulans*; and Dy, *D. yakuba*). The positions correspond to the first amino acid (aa) of the *Dm* SMO. Conserved serine (S) and threonine (T) are in red, and the stripes indicate a region with no conserved S or T. PKA/CKI phosphorylation clusters are conserved (dark gray box, with the residues phosphorylated by the PKA underlined). Some conserved S and T are clustered in four groups (GI, II, III and IV) in the C-terminal. Binding to FU was reported to occur between aa 985 and 1036 (Malpel et al., 2007). SMO variants used in this study are shown below, where conserved S or T residues were substituted by alanine (A) or by aspartic acid (D) in the PKA/CKI cluster and/or Ct clusters. (B-F) Immunodetection of various forms of transiently transfected SMO-HA in extracts of Cl8 cells with an antibody against HA (αHA). (B) SMO^{wt}-HA (lanes 1 and 2), $SMO^{Ct\text{-}SA}$-HA (lanes 3 and 4), $SMO^{PKA\text{-}SA}$-HA (lanes 5 and 6), $SMO^{PKA\text{-}SA\ Ct\text{-}SA}$-HA (lanes 7 and 8) without (–) or with (+) HH. Here and in the following blots, the bracket indicates the phosphorylated forms of SMO-HA with a slower migration and GMAP is used as loading control. (C) SMO^{wt}-HA (lanes 1 and 2), $SMO^{PKA\text{-}SA}$-HA (lanes 3 and 4) and $SMO^{PKA\text{-}SA\ Ct\text{-}SA}$-HA (lanes 5 and 6) without (–) or with (+) GAP-gFU. Here and in (D-F), the presence of GAP-gFU is verified by immunoblotting with an antibody against GFP (αGFP). (D) SMO^{wt}-HA (lanes 1-3), $SMO^{Ct\text{-}SA}$-HA (lanes 4-6) without (–) (lanes 1 and 4) or with GAP-gFU (lanes 2 and 5) or GAP-cFU-DANA (lanes 3 and 6), a kinase dead form of GAP-FU. (E) $SMO^{PKA\text{-}SD}$-HA (lanes 1-4), $SMO^{PKA\text{-}SD\ Ct\text{-}SA}$-HA (lanes 5-8) alone (lanes 1 and 5), with GAP-gFU (lanes 3 and 7) or with GAP-cFU-DANA (lanes 4 and 8); in the absence (lanes 1 and 5) or presence (lanes 2-4 and 6-8) of HH. Note that the shift of $SMO^{PKA\text{-}SD}$ was not totally suppressed by GAP-cFU-DANA, probably because of the phosphorylation of sites other than the Ct-sites. (F) SMO^{wt}-HA (lanes 1 and 2), $SMO^{PKA\text{-}SD}$-HA (lanes 3 and 4), $SMO^{PKA\text{-}SD\ Ct\text{-}SA}$-HA (lanes 5 and 6) without (–) or with (+) GAP-gFU. Note that tagging SMO to its N-terminal was shown to preserve its function (Zhu et al., 2003). The asterisk indicates multimeric forms of SMO. (G) Immunodetection of SMO in extracts of wing imaginal disc from *MS1096* (expressing GAL4 in the whole wing pouch), *MS1096; UAS* smo^{wt}, *MS1096; UAS* $smo^{Ct\text{-}SA}$ and *MS1096; UAS* $smo^{Ct\text{-}SD}$ flies, respectively. In *MS1096* control discs (lane 1), only phosphorylated forms of SMO (pSMO) are visible. In discs that express the smo^{wt} transgene (lane 2), the levels of both forms of SMO (p-SMO and SMO) are increased. In comparison, $SMO^{Ct\text{-}SA}$ (lane 3) was less phosphorylated than SMO^{wt}, as shown by the reduced pSMO/SMO ratio, especially considering the contribution of endogenous SMO to pSMO. By contrast, $SMO^{Ct\text{-}SD}$ (lane 4) is mainly present as a phosphorylated form. Red and black arrowheads indicate hyperphosphorylated (pSMO) and non-phosphorylated (SMO) forms of SMO, respectively. TUB, tubulin used as a loading control. All the western blots in all figures have been performed in at least three independent replicates.

Development (2017) 144, 1841-1850 doi:10.1242/dev.144782

the absence of HH, whereas SNAP-SMO$^{PKA\text{-}SD\ Ct\text{-}SD}$ was constitutively accumulated at very high levels, reaching almost fourfold those of SNAP-SMO$^{PKA\text{-}SD}$.

We therefore conclude that the phosphorylation of the Ct-sites strongly enhances the stabilizing effects of the phosphorylation of PKA/CKI sites induced by HH.

Phosphorylation of the Ct-sites increases SMO localization at the plasma membrane

We then examined whether the subcellular localization of SMO was regulated by the phosphorylation of its Ct-sites. The cell surface and intracellular pools of SNAP-SMO were differentially marked by sequentially using membrane impermeable and permeable SNAP substrates carrying different fluorophores (Fig. 2D-F; Fig. S3). As expected, HH stimulation led to accumulation of SNAP-SMO^{wt} at the plasma membrane. This initial experiment also revealed two important features. First, all the hyperphosphorylated forms of SMO are at the cell surface and, reciprocally, the intracellular pool of SMO lacks extensive phosphorylation. Second, HH stimulation mainly induced an increase in the levels of SNAP-SMO^{wt} at the cell surface, whereas intracellular levels were almost unaffected. By contrast with SNAP-SMO^{wt}, SNAP-SMO$^{Ct\text{-}SA}$ stayed intracellular even in the presence of HH. Moreover, in the absence of HH, SNAP-SMO$^{Ct\text{-}SD}$ displayed a weak but significant increased (twofold) localization to the plasma membrane, which was strongly enhanced by HH (15-fold). As expected, SNAP-SMO$^{PKA\text{-}SA}$ remained intracellular in the presence of HH, whereas SNAP-SMO$^{PKA\text{-}SD}$ was mostly at the plasma membrane even in the absence of HH. This latter effect was suppressed in SNAP-SMO$^{PKA\text{-}SD\ Ct\text{-}SA}$ but was further increased in SNAP-SMO$^{PKA\text{-}SD\ Ct\text{-}SD}$.

We conclude that phosphorylation of the Ct-sites is required for the accumulation of high levels of SMO at the cell surface promoted by the phosphorylation of the PKA/CKI clusters in response to HH.

Phosphorylation of SMO Ct-sites controls its apicobasal distribution

SNAP labeling was then used to analyze the effects of Ct-site phosphorylation on the subcellular distribution of SMO *in vivo*. Wing imaginal discs expressing SNAP-tagged forms of SMO in the dorsal compartment were labeled with a membrane impermeable SNAP ligand. The ventral compartment served as an internal negative control. Labeled SNAP-SMO thus corresponds to molecules that were – at least transiently – present at the plasma membrane during the labeling time. In agreement with the Cl8 data, labeled SNAP-SMO^{wt} was at higher levels both at the plasma membrane and in intracellular vesicles in HH sending posterior cells and in A/P receiving cells (Fig. 3A). By contrast, SNAP-SMO$^{Ct\text{-}SA}$ was less labeled and mostly present in intracellular vesicular structures, whereas SNAP-SMO$^{Ct\text{-}SD}$ was highly labeled, with an enrichment at the plasma membrane of the HH sending and receiving cells (Fig. 3B,C). We also observed distinctions in labeled SNAP-SMO^{wt} distribution along the apicobasal axis of the wing epithelium (Fig. 3D): labeled SNAP-SMO^{wt} was present at the apical side (visualized with aPKC staining) of the P cells and of the A cells that receive HH and also in the most basal region of the P cells and of the A cells abutting A/P in the region where the highest levels of HH are encountered. This basal distribution was lost with labeled SNAP-SMO$^{Ct\text{-}SA}$ and increased with labeled SNAP-SMO$^{Ct\text{-}SD}$, indicating that it is dependent on the phosphorylation of the Ct-sites (Fig. 3E,F). Note that these effects were also seen by immunofluorescence with untagged SMO variants (Fig. S4).

In summary, the phosphorylation of the Ct-sites regulates the subcellular localization of SMO in response to HH by two means: (i) it increases its accumulation at the plasma membrane; and (ii) it promotes its localization in the basal region of the polarized epithelial cells of the wing imaginal disc.

Phosphorylation of the SMO Ct-sites upregulates its activity *in vivo*

We then assayed whether the phosphorylation of the Ct-sites regulates SMO activity. SMO^{wt}, SMO$^{Ct\text{-}SA}$ and SMO$^{Ct\text{-}SD}$ were expressed in the D compartment, and HH signaling was monitored by following CI-FL and PTC accumulation. Despite some variation, clear signatures specific to the different forms of SMO were observed (Fig. 3G-K). SMO^{wt} overexpression led to a mild upregulation of HH signaling as indicated by: (1) an upregulation of CI-FL levels at the A/P boundary (in >50% of discs) and its ectopic accumulation in the A part of the wing discs (in >65% of discs; Fig. 3G1,J); and (2) an increase in PTC levels at the A/P border (in >60% of discs) and its occasional ectopic expression towards the anterior (20% of discs; Fig. 3G2,K). By contrast, SMO$^{Ct\text{-}SA}$ tended to decrease HH signaling (Fig. 3H,J,K). It never led to ectopic PTC and led to ectopic CI-FL accumulation about four times less often than SMO^{wt}. Moreover, it downregulated PTC levels and/or CI-FL in almost 30% of discs, two events rarely seen with SMO^{wt} expression. Conversely, expression of SMO$^{Ct\text{-}SD}$ led to a stronger activation of HH signaling than SMO^{wt}, with an enhanced accumulation of CI-FL and PTC in the whole A compartment in 80 and 72% of the discs, respectively (Fig. 3I-K).

Together, these results indicate that the phosphorylation of the Ct-sites of SMO upregulates its activity.

Phosphorylation of the SMO Ct-sites enhances the activating effects of phosphorylation at the PKA/CKI sites

For better assessment of the roles of the phosphorylation of Ct-sites, we analyzed the impact of mutating them on SMO$^{PKA\text{-}SD}$ activity. SMO$^{PKA\text{-}SD}$ is known to be active constitutively (Jia et al., 2004), and its expression in the wing pouch led to an increased expression of all known HH targets (Fig. 4; Fig. S5). This was associated with an increase in CI-FL levels throughout the A compartment, with an enlargement of the region near the A/P boundary that normally displays low levels of CI-FL (corresponding to CI-A and therefore called the 'CI-A region') owing to the presence of high levels of HH. All these effects were stronger with SMO$^{PKA\text{-}SD\ Ct\text{-}SD}$, with a very strong ectopic *en* expression and an important enlargement of the CI-A region. By contrast, SMO$^{PKA\text{-}SD\ Ct\text{-}SA}$ led to CI-FL accumulation in the A region but it was unable to promote ectopic target gene expression. Moreover, *en* expression at the A/P boundary was suppressed along with the CI-A region, and *col* and *ptc* expression were strongly downregulated. However, the expression domains of the 'low HH' responsive genes *dpp* and *iroquois* (*iro*) were almost normal. Notably, these negative effects of SMO$^{PKA\text{-}SD\ Ct\text{-}SA}$ are also seen in the absence of endogeneous SMO protein (see Fig. S6).

In conclusion, phosphorylation of the Ct clusters is required for the constitutive activity of SMO$^{PKA\text{-}SD}$ and enhances its effects. By contrast, preventing Ct cluster phosphorylation in SMO$^{PKA\text{-}SD}$ blocks the response to high levels of HH but has almost no effect on the target genes that respond to low HH levels.

Development (2017) 144, 1841-1850 doi:10.1242/dev.144782

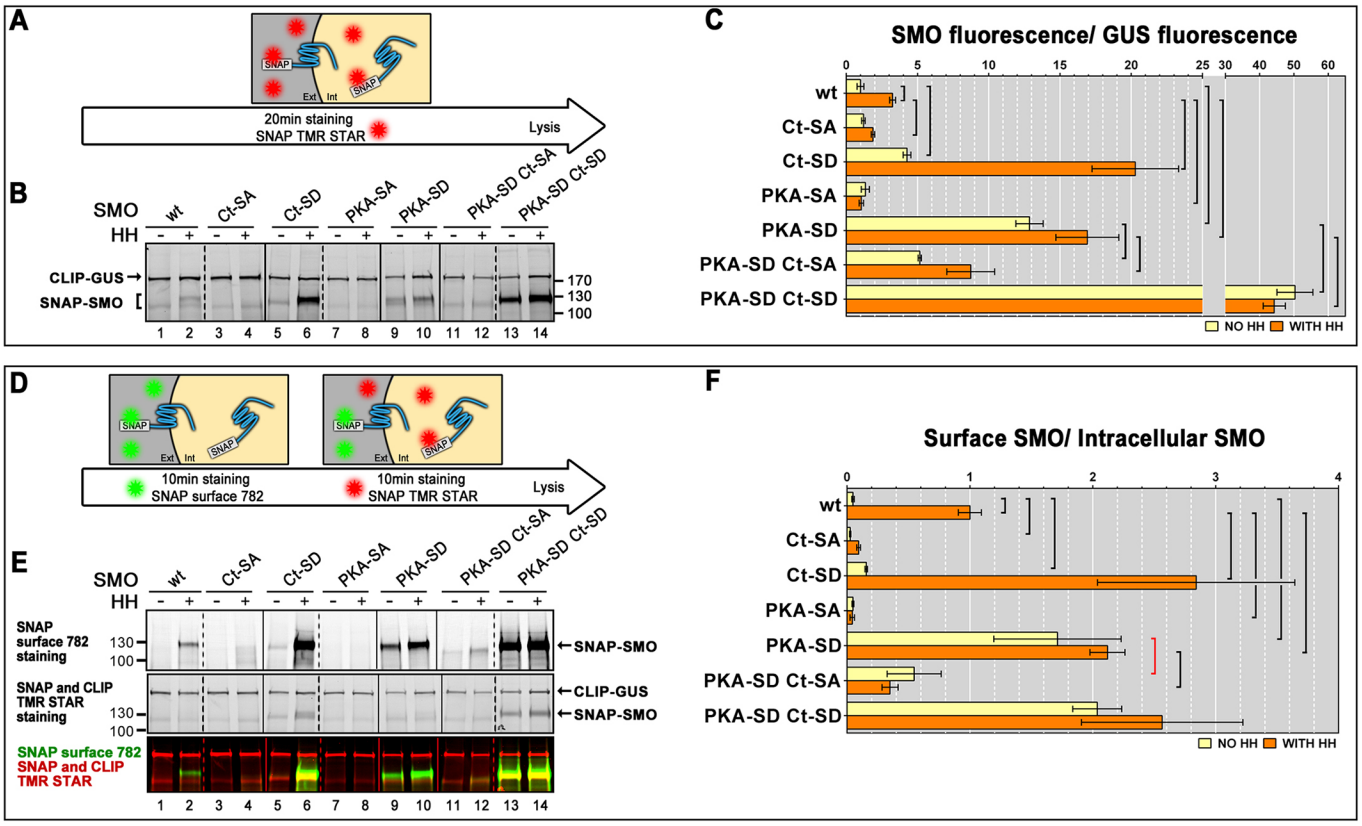

Fig. 2. Phosphorylation of the Ct-sites controls the levels of SMO at the plasma membrane. (A) Transfected Cl8 cells expressing the different SNAP-SMO constructs were labeled for 20 min with a permeable fluorescent substrate (TMR STAR) that marked both cell surface and intracellular SNAP-SMO. Extracellular (Ext) in gray and intracellular (Int) in yellow. (B) Representative fluorescent scanning of extracts of cells labeled as indicated in (A) and cotransfected with various forms of SNAP-SMO along with CLIP-GUS, which is a fusion between the *Escherichia coli* glucoronidase (*GUS*) gene and the CLIP-tag, a derivative form of SNAP-tag with different substrate specificity. Here and in (E), CLIP-GUS was used as an internal control for experimental variations including the ones attributable to transfection efficiency variation. (C) Graph showing the ratio between the amounts of SNAP-SMO and those of CLIP-GUS (in arbitrary units). The variants of SMO tested are indicated, and the value for SNAP-SMO^{wt} in the absence of HH was taken as the reference (=1). Here and in (F), yellow is without HH and orange with HH; quantifications are from three biological replicates that were scanned together. Gel images in (B) and (E) are composites of representative results (the dashed lines indicate when the samples were on the same gel and the continuous lines when they came from gels run in parallel and treated in the same conditions). In (C) and (F), the error bars represent the s.d. Statistical analysis by one tailed bivariate Wilcoxon rank tests: black bracket, P=0.05; red bracket, P=0.1. (D) Transfected Cl8 cells expressing the SNAP-SMO constructs were labeled for 10 min with a non-liposoluble 782 nm fluorescent substrate (SNAP surface 782) that could not pass through the membrane and therefore labeled only the population of SMO molecules present at the cell surface. Then, the cells were labeled for 10 min with a membrane permeable fluorescent substrate (SNAP TMR STAR) before being lysed. (E) Representative fluorescent scanning of extracts of transfected Cl8 cells cotransfected with various forms of SNAP-SMO along with CLIP-GUS and labeled as indicated in (D). Fluorescent SNAP surface staining is shown in the upper panel and fluorescent SNAP and CLIP TMR staining in the middle panel. A merged image of the two stainings is shown in the lower panel. Images of corresponding intact cells are shown in Fig. S3. (F) Ratio of the cell surface to the intracellular fluorescence obtained with different forms of SNAP-SMO. The values were normalized to the ratio obtained for SNAP-SMO^{wt} in the presence of HH.

The negative effects of SMO$^{PKA\text{-}SD\ Ct\text{-}SA}$ are suppressed by activated FU

Strikingly, the expression of SMO$^{PKA\text{-}SD\ Ct\text{-}SA}$ phenocopies the effects of mutations disrupting FU kinase activity. In *fu* mutants altered in the kinase domain, *en* and *col* expression are strongly reduced, inactive CI-FL accumulates and the CI-A region disappears, whereas *dpp* is almost unaffected (Alves et al., 1998). It might thus be the case that SMO$^{PKA\text{-}SD\ Ct\text{-}SA}$ traps or freezes endogenous FU in an inactive state. This prompted us to examine the consequences of SMO$^{PKA\text{-}SD\ Ct\text{-}SA}$ expression on the three proteins whose phosphorylation depends on FU activity and are likely targets of FU: COS2, FU itself and its antagonist, SU(FU). Myc-tagged versions of these proteins were transiently coexpressed with SMO^{wt}-HA in Cl8 cells (Fig. 5A). All three displayed low levels of phosphorylation (visualized by a shift in their electrophoretic migration) in the presence of SMO^{wt} and HH. Consistent with their signaling activity, SMO$^{Ct\text{-}SA}$-HA and SMO$^{Ct\text{-}SD}$-HA led to a slight (but reproducibly) reduced and increased phosphorylation, respectively. As expected, SMO$^{PKA\text{-}SD}$ also upregulated their phosphorylation in the absence of HH. By contrast, SMO$^{PKA\text{-}SD\ Ct\text{-}SA}$ expression prevented (COS2 and FU) or reduced [SU(FU)] phosphorylation, both in the absence and in the presence of HH. This indicates that SMO$^{PKA\text{-}SD\ Ct\text{-}SA}$ negatively affects the kinase activity of endogenous FU.

To test this possibility further, we examined whether the negative effects of SMO$^{PKA\text{-}SD\ Ct\text{-}SA}$ were rescued by the expression of GAP-CFP-FU (GAP-cFU; Fig. 5B-E; Fig. S7). As previously reported, GAP-cFU expression led to an activation of the pathway, with ectopic *ptc*, *col* and *dpp* expression and ectopic accumulation of CI-FL. When GAP-cFU was coexpressed with SMO$^{PKA\text{-}SD\ Ct\text{-}SA}$, all HH targets were ectopically expressed. Surprisingly, these effects were stronger than those of GAP-cFU or SMO$^{PKA\text{-}SD\ Ct\text{-}SA}$ alone as indicated by high levels of ectopic *en* expression throughout the

Development (2017) 144, 1841-1850 doi:10.1242/dev.144782

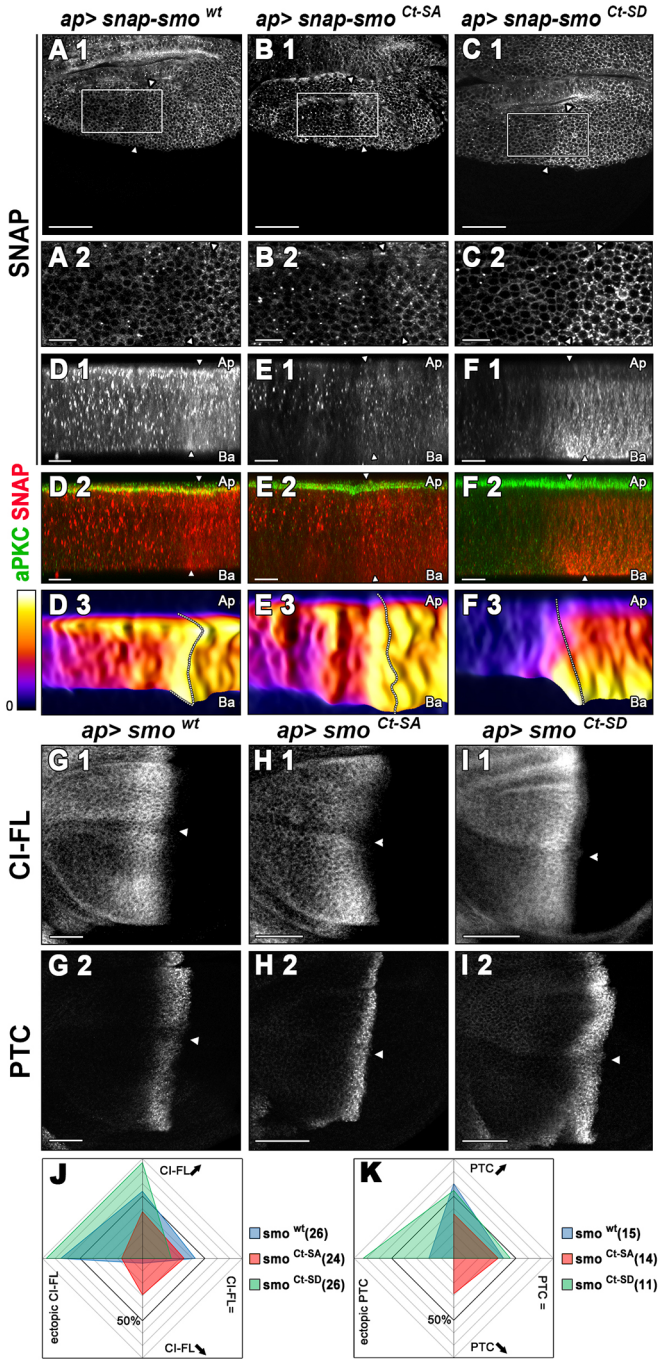

Fig. 3. Phosphorylation of the Ct-sites controls SMO localization and activity *in vivo*. (A-F) XY confocal images (A-C) or XZ confocal images (D-F) of wing discs expressing *UAS snap-smo*^{wt} (A,D), *UAS snap-smo*$^{Ct\text{-}SA}$ (B,E) and *UAS snap-smo*$^{Ct\text{-}SD}$ (C,F) driven by *apGal4* and labeled with a non-liposoluble fluorescent substrate (A-F) and stained with aPKC (green; D2-F2). The XZ sections are perpendicular to the A/P axis through the dorsal compartment. The images in (D3-F3) show the distribution of SNAP-SMO forms along the apicobasal axis in three-dimensional false color. The rectangle in (A1-C1) corresponds to the region enlarged in (A2-C2). The A/P boundary (determined by CI-FL staining, not shown) is indicated either by two arrowheads or by a dotted line. Ap, apical; Ba, basal. Note that the imaging conditions used optimized the acquisition of SMO for each genotype. The XZ images correspond to maximal intensity projection from 13 sections. Here and in the following figures, XY disc images are oriented dorsal up and anterior left. (G-I) Representative XY confocal images of wing discs of *apGAL4* flies expressing *UAS smo*^{wt} (G), *UAS smo*$^{Ct\text{-}SA}$ (H) and *UAS smo*$^{Ct\text{-}SD}$ (I) and stained with antibodies against CI-FL (G1-I1) or PTC (G2-I2). The white arrowhead indicates the position of the dorsoventral boundary. (J,K) For each labeling, the discs were classified in a blind experiment according to four phenotypic criteria that reflect the strength of HH activation: decreased accumulation at A/P (down arrow), no effect on accumulation at A/P (=), increased accumulation at A/P (up arrow) and ectopic accumulation (ectopic). The percentage of the different phenotypes observed for each genotype is presented on the radar diagram for CI-FL (J) and for PTC (K) staining. The number of discs analyzed is indicated in brackets. Scale bars: 50 µm in A1,B1, C1,G,H,I; 20 µm in the other panels.

entire A compartment. Notably, CI-FL levels were strongly reduced, presumably because of the generation of the CI-A form throughout the A compartment.

These data show that the expression of an active form of FU can totally suppress the negative effects of SMO$^{PKA\text{-}SD\ Ct\text{-}SA}$ on the 'high HH' targets and that, reciprocally, its effects on all HH targets are increased by SMO$^{PKA\text{-}SD\ Ct\text{-}SA}$.

DISCUSSION

We identified new phosphorylations of the fly SMO cyto-tail and showed that they are promoted by the protein kinase FU. This phosphorylation is part of a multisite, multikinase phosphorylation cascade, which controls both SMO accumulation at the plasma membrane and its distribution along the apicobasal axis. These phosphorylation events participate in amplification feedback loops, which promote high levels of SMO-FU activation that allow responses to high doses of the HH signal.

Multisite, multikinase phosphorylation of SMO

Several kinases are involved in SMO cyto-tail hyperphosphorylation, including PKA/CKI, CKII, aPKC, GPRK2/GRK2 and CK2γ/Gish. Here, we identify four new phosphorylation clusters in its most C-terminal part, near the FU binding site, that are required for the full phosphorylation of SMO in response to HH. FU might act on SMO phosphorylation directly or indirectly through the recruitment, increased expression (via CI activation) or activation of another kinase. Although definite proof of a direct effect is lacking in the absence of an *in vitro* FU kinase assay, several lines of evidence support that possibility, as follows: (i) blocking endogenous FU activity by a dominant negative form reduces the HH induced phosphorylation of SMO; (ii) expressing a form of FU that is not anchored to the plasma membrane also promotes SMO phosphorylation (although less efficiently than GAP-FU); (iii) both GAP-gFU-kinase activity and its interaction with SMO are required for GAP-gFU to promote the phosphorylation of Ct-sites; and (iv) the induction of SMO phosphorylation by FU or GAP-FU on SMO is also seen with S2 cells that fail to express CI. Note also that FU might act on only a few of these sites, which would prime the phosphorylation of adjacent sites by another kinase, as shown for its own autophosphorylation (Zhou and Kalderon, 2011).

Our data also suggest that sequential phosphorylation of SMO initiated at the PKA/CKI sites leads to the phosphorylation of the Ct-sites. This could be attributable to the conformational changes induced by the PKA/CKI phosphorylation, which could increase the accessibility of the Ct-sites. Alternatively, the phosphorylation of the PKA/CKI sites could act indirectly by promoting FU activation. We favor this latter possibility for the following reasons: (i) FU can be directly activated by SMO (Claret et al., 2007; Zhou and Kalderon, 2011); and (ii) GAP-gFU can promote the phosphorylation of SMO^{wt} in the absence

Development (2017) 144, 1841-1850 doi:10.1242/dev.144782

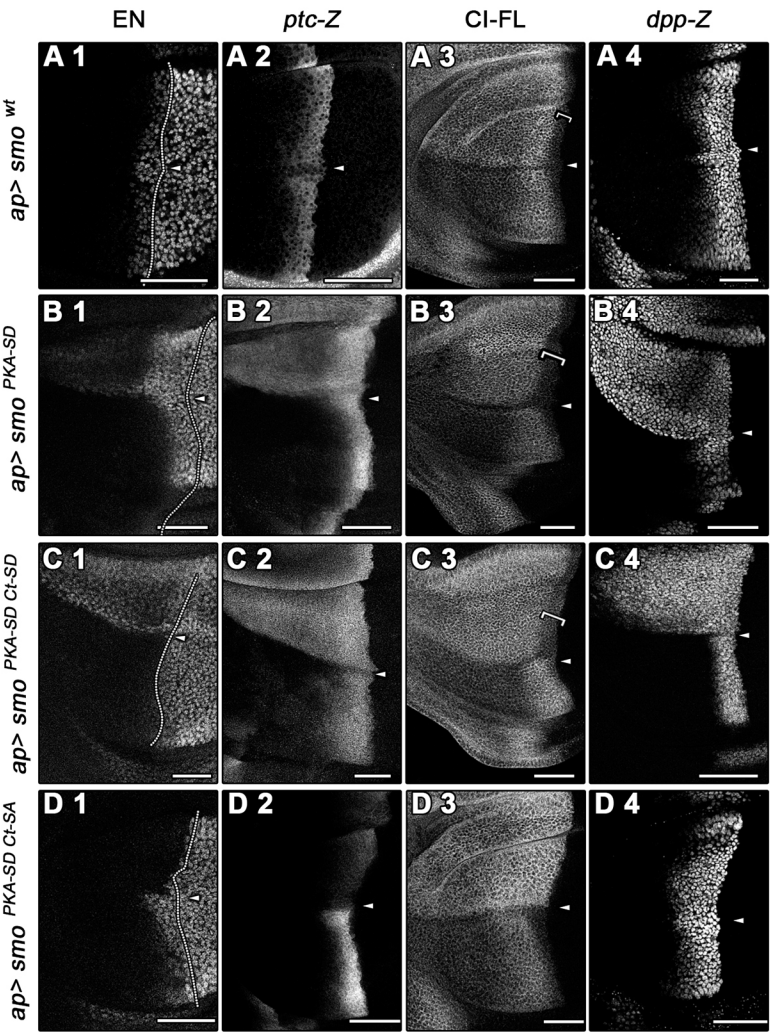

Fig. 4. Phosphorylation of the Ct-sites increases the effects of PKA/CKI phosphorylation. (A-D) Wing discs expressing *UAS* smo^{wt} (A), *UAS* $smo^{PKA\text{-}SD}$ (B), *UAS* $smo^{PKA\text{-}SD\ Ct\text{-}SD}$ (C) and *UAS* $smo^{PKA\text{-}SD\ Ct\text{-}SA}$ (D) in the dorsal compartment using *apGAL4* and stained with antibodies against EN (A1-D1), β-galactosidase (*ptc-Z*) to follow *ptc-Z* (A2-D2) or *dpp-Z* transcriptional fusion reporters (a4-d4) and CI-FL (A3-D3). A slight expansion of the dorsal expression domain of *dpp* is observed when $smo^{PKA\text{-}SD\ Ct\text{-}SA}$ is expressed. This is probably attributable to further spreading of HH resulting from the strong reduction of PTC at the A/P boundary. The brackets in A3-C3 indicate the reduced accumulation of CI-FL near the A/P boundary associated with its high activation state. Scale bars: 50 µm. At least 20 discs per phenotype were analyzed.

of phosphorylation of the PKA/CKI sites of SMO (Claret et al., 2007; and present study).

SMO localization and levels

SMO phosphorylation by PKA/CKI is necessary and sufficient to promote an increase in SMO levels and its localization at the plasma membrane, but the temporal, spatial and functional connections between these events remain elusive. Several scenarios can be considered. For instance, SMO phosphorylation could block SMO endocytosis once it has reached the cell surface or it could upregulate the targeting of newly synthesized SMO to the plasma membrane. Our data, in agreement with (Kupinski et al., 2013), strongly support the first hypothesis, as follows: (i) the increase of SMO induced by HH, by the phosphorylation of its PKA/CKI sites, or both, is almost entirely attributable to an increase of its cell surface pool, with only very modest effects on intracellular SMO levels; and (ii) the phosphorylated SMO molecules are entirely located at the cell surface and, reciprocally, all of the cell surface fraction is phosphorylated.

Moreover, the phosphorylation of the Ct-sites seems to act by increasing the effects of the PKA/CKI sites on the stabilization of SMO at the plasma membrane. Mimicking the phosphorylation of the Ct-sites leads to a strong increase of the fraction of SMO present at the plasma membrane, and this effect is most visible either in the presence of HH – when the PKA/CKI sites are phosphorylated – or when their phosphorylation is mimicked.

SMO activation

Phosphorylation of the PKA/CKI sites increases SMO activity by antagonizing a region called the SMO auto-inhibitory domain (SAID), which shuts down SMO activity in the absence of HH, owing to its intermolecular electrostatic interaction with acidic aa of the most C-terminal region of SMO (Zhao et al., 2007). As a result, the SMO cyto-tail dimerizes. This effect is increased by GPRK2/GRK2 phosphorylation (Maier et al., 2012). By contrast, FU acts on sites located in or near the acidic region, and their phosphorylation further increases the negative charges in this region, which suggests that they might activate SMO by a new (so far, not understood) mechanism. Nonetheless, the effects of phosphorylation of Ct-sites strengthen the tight correlation between SMO signaling activity and its accumulation at the cell surface, and they further support the notion that the concentration or number of SMO molecules present at the cell surface is crucial for HH signaling. Finally, the phosphorylation of the Ct-sites of SMO appears also to be involved in the apicobasal localization of SMO, leading to increased basal localization in the HH receiving cells. Although the significance of this differential localization awaits further experimentation, it is interesting to consider it in the light of the double HH gradient that has been described: apical for the long range, 'low HH' responses and basal for the short range, 'high HH' responses (for review, see Guerrero and Kornberg, 2014).

Development (2017) 144, 1841-1850 doi:10.1242/dev.144782

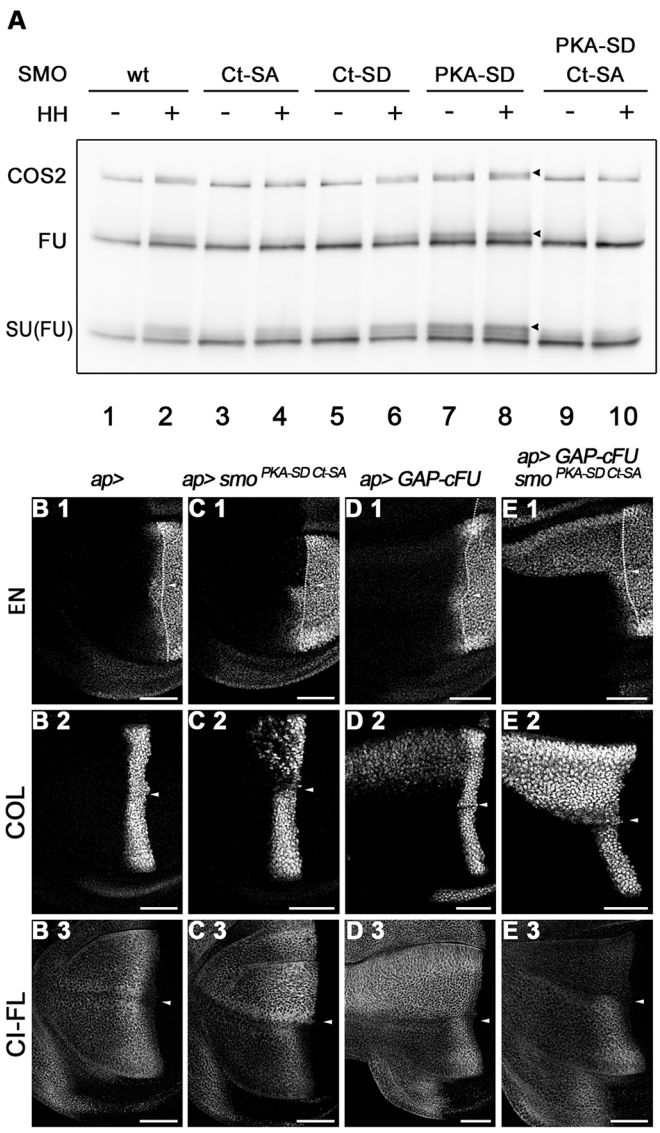

Fig. 5. The negative effects of SMO$^{PKA\text{-}SD\ Ct\text{-}SA}$ are suppressed by coexpression of constitutively active FU. (A) Immunodetection of myc-COS2, myc-FU and SU(FU)-myc in extracts of Cl8 cells coexpressing SMO^{wt}-HA (lanes 1 and 2), SMO$^{Ct\text{-}SA}$-HA (lanes 3 and 4), SMO$^{Ct\text{-}SD}$-HA (lanes 5 and 6), SMO$^{PKA\text{-}SD}$-HA (lanes 7 and 8) and SMO$^{PKA\text{-}SD\ Ct\text{-}SA}$-HA (lanes 9 and 10) without (–) or with (+) HH. Arrowheads indicate the most phosphorylated forms of myc-COS2, myc-FU and SU(FU)-myc. (B-E) Wing discs of *apGAL4* flies (B) or expressing *UAS smo*$^{PKA\text{-}SD\ Ct\text{-}SA}$ (C), *UAS GAP-cFU* (D) and *UAS GAP-cFU* with *UAS smo*$^{PKA\text{-}SD\ Ct\text{-}SA}$ (E) and stained with antibodies against EN (B1-E1), COL (B2-E2) and CI-FL (B3-E3). Expression of GAP-cFU led to anterior expansion of the expression of *col* and *en* and to an ectopic accumulation of CI-FL. Coexpression of GAP-cFU and *smo*$^{PKA\text{-}SD\ Ct\text{-}SA}$ led to ectopic expression of all HH targets. Note that the effects of GAP-cFU overexpression were further enhanced in the presence of SMO$^{PKA\text{-}SD\ Ct\text{-}SA}$ and that GAP-cFU has a mild effect compared with previous published data (Claret et al., 2007) owing to lower expression levels. Scale bars: 50 µm. Note that SMO$^{PKA\text{-}SD}$ also increases the effect of GAP-cFU (Fig. S8).

Function and regulation of the kinase FU

Both phosphorylation of SMO Ct-sites and FU kinase activity are necessary for high levels of HH signaling and for the increase in SMO levels and cell surface localization induced by HH (Claret et al., 2007; Liu et al., 2007). So far, these effects have been attributed to the ability of FU to phosphorylate COS2 and SU(FU). Our results provide a new output for FU as they show that it is likely to upregulate the levels of SMO directly at the cell surface and its signaling activity by phosphorylation. It is noteworthy that the FU-dependent phosphorylation of COS2 has been recently shown not to be essential for its activity as SMO and COS2 interact (Zadorozny et al., 2015); it is thus possible that the effect of FU on COS2 activity could in fact occur mainly via SMO. Our work also reveals that the FU downstream activity [i.e. the phosphorylation of SU(FU) and COS2] requires the phosphorylation of SMO Ct-sites. It indicates that SMO activates FU in a two-step mechanism: (i) an initial activation of FU by recruitment to the plasma membrane and that promotes its action on SMO; and (ii) a second step that requires the phosphorylation of SMO Ct-sites, which is necessary for FU effects on its cytosolic targets and the activation of CI-FL.

FU/SMO mutual activation controls high levels of HH signaling

These results provide evidence of the interplay between SMO and FU which, by increasing SMO phosphorylation, leads to high SMO/FU activation. We propose a model whereby SMO/FU activation is based on the progressive multisite phosphorylation of SMO and on a series of activation loops that take place between SMO and FU in the presence of high levels of HH (Fig. 6). This amplifying loop finally leads to a high accumulation of the hyperactivated SMO/FU couple at the cell surface, reaching a threshold of activation sufficient to promote high levels of CI activation and the 'high HH' specific responses. Interestingly, multisite phosphorylation can lead to ultrasensitivity under some circumstances and to bistability when combined with a positive feedback loop (for review, see Ferrell and Ha, 2014a,b; Lander, 2007). In this context, the crosstalk between SMO and FU might provide both robustness and switch-like behavior to the HH pathway that could account in part for its morphogenetic effects. Although SMO has been conserved from flies to mammals, significant differences have appeared between human and fly SMO and its regulation (Ingham et al., 2011). This has probably led to some changes in the molecular mechanism, but the underlying principles of the regulation might well have been conserved.

MATERIALS AND METHODS

Drosophila strains and genetics

For transgenesis, wild-type and mutants *smo* cDNAs were introduced into the same landing site (9738) on 3R (at 99F8) by BestGene, using the *PhiC31* integration system. For MARCM clones, the larvae were heat-shocked 3-4 days after egg laying for 2 hours at 37°C. Further details are given in the supplementary Materials and Methods.

Immunostaining of imaginal discs

Discs were dissected and treated as described by Claret et al. (2007) with minor modifications (see supplementary Materials and Methods). The primary antibodies used were: mouse anti-PTC, 1:1000 [Apa 1, from Developmental Studies Hybridoma Bank (DHSB)] (Martin et al., 2001); mouse anti-SMO, 1:100 (20C6, from DSHB) (Lum et al., 2003); mouse anti-COL, 1:100 (a gift from M. Crozatier, Center for Integrative Biology, Toulouse, France) (Crozatier et al., 2003); rat anti-full length CI, 1:5 [2A1 from R. Holmgren, Northwestern University, Evanston, IL, USA (Motzny and Holmgren, 1995)]; and rabbit polyclonal anti-β-galactosidase 1/100 (ABR, Affinity BioReagents).

Plasmids

All expression vectors were constructed by the Gateway recombination method (Invitrogen) and checked by sequencing the mutated regions. Details of the constructs used here are presented in the supplementary Materials and Methods.

Development (2017) 144, 1841-1850 doi:10.1242/dev.144782

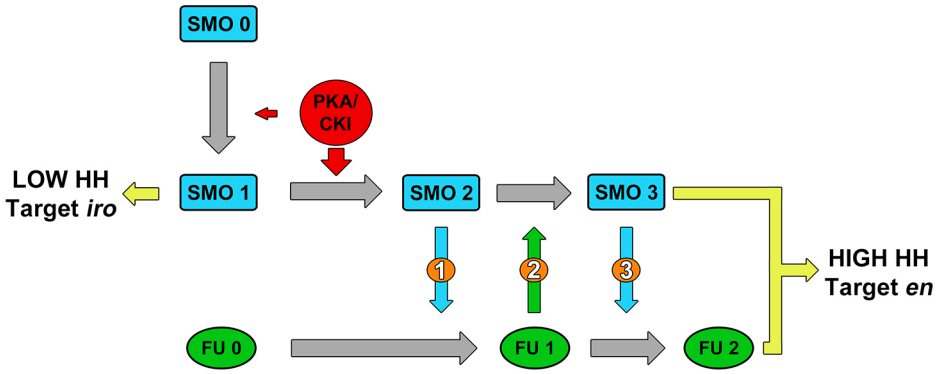

Fig. 6. Model: SMO/FU act as a molecular switch that participates in high levels of HH signaling. HH gradient promotes graded phosphorylation of the PKA/CKI sites of SMO, leading to a progressive increase of SMO levels and an increase in CI-FL. At low concentrations of HH, PKA/CKI leads to a low activity of SMO (called SMO 1) sufficient to block CI processing, leading to the expression of 'low HH' targets, such as *dpp* and *iro*. Higher levels of HH lead to increased SMO phosphorylation, and SMO (called SMO 2) reaches a threshold of activation sufficient to promote the activation of FU (FU 1; step 1). In turn, activated FU phosphorylates (directly or indirectly) SMO on its Ct-sites (step 2), leading to higher levels of SMO activity (SMO 3) that allow further FU activation (FU 2; step 3) and action on its downstream targets. As a result, high levels of the hyperactive SMO/FU (SMO 3/FU 2) pair are accumulated at the plasma membrane and allow very high levels of HH signaling associated with the accumulation of low levels of CI-A, which controls 'high HH' targets, such as *en*. SMO/FU 0, 1 and 2 (and 3 for SMO) represent increasing levels of SMO or FU activation, respectively.

CI8 cell culture, transfection and western blotting

Cl-8 cells were cultured as described previously (Claret et al., 2007). Transient transfections were then carried out using Transit Insect Reagent (Mirus) and analyzed 48 h post transfection. Note that to visualize SMO protein, the samples were not heated. The samples were run on 10% Anderson gels. See supplementary Materials and Methods for more details.

CI8 SNAP labeling experiments

Forty-eight hours after transfection, cells were washed in PBS then either labeled for 20 min in complete cell medium with 0.75 µM SNAP TMR-star and 0.75 µM CLIP TMR-star (NEB) for total SMO accumulation or labeled for 10 min with 0.75 µM SNAP-Surface 782 in complete cell medium, before adding 0.75 µM SNAP TMR-star and 0.75 µM CLIP TMR-star for 10 min for surface and intracellular staining. In both cases, cells were then washed twice and lysed in 1% NP-40, 150 mM NaCl, 50 mM Tris, 1 mM dithiothreitol with complete EDTA-free antiprotease mix (Roche) and Phosphatase Inhibitor Cocktail Set II (Calbiochem). The lysate was centrifuged (12,000 ***g***) for 10 min at 4°C and mixed with Laemmli sample buffer (Bio-Rad) and 0.1 M dithiothreitol. Fifteen microliters of each sample was loaded on precast 4-20% Mini-Protean TGX gels (Bio-Rad) and run as for western blots (see supplementary Materials and Methods). Gels were scanned either on a Typhoon Trio imager (GE Healthcare; excitation 532 nm, emission 580 nm, PMT 700 V) for total accumulation or sequentially (for surface and intracellular staining) on a Lycor Odyssey at 800 nm before Typhoon Trio. The merged image was obtained by overlapping the two images. Three independent experiments (with all the constructs together) were performed. All gels were run and scanned together. Images were analyzed and quantified using ImageJ software. One tailed bivariate Wilcoxon rank tests were run using R software and R Commander (R Foundation for Statistical Computing).

Wing discs SNAP labeling experiments

Third instar larva were dissected in S2 cell medium. They were then incubated for 30 min with the nonliposoluble Alexa 546 fluorescent substrate at a dilution of 1/600 in S2 medium to allow fixation of the substrate and then incubated for 10 min at 25°C. The larvae were fixed 20 min with PFA, followed by three 10 min washes (PBS with 0.3% Triton) before immunostaining or direct imaging.

Acknowledgements

We thank M. Crozatier, J. Jiang, D. Kalderon, T. Kornberg, S. Ogden, D. Robbins, P. Thérond, A. Zhu and their laboratories for flies and reagents. We are grateful to F. Schweisguth, L. Ruel, G. D'Angelo, P. Therond, A. Brigui and our colleagues from the Institut Jacques Monod for insightful discussions and to T. Herbillon for technical help. Antibodies from the DSHB were developed under the auspices of the NICHD and maintained by the University of Iowa. *Drosophila* embryo injections were carried out by BestGene Inc. We acknowledge the ImagoSeine core facility of Institut Jacques Monod, member of France-BioImaging (ANR-10-INBS-04) and certified IBiSA.

Competing interests

The authors declare no competing or financial interests.

Author contributions

Conceptualization, M.S., I.B., L.H., R.A.H. and A.P.; methodology, M.S. and I.B.; validation, M.S. and I.B.; formal analysis, M.S., I.B., L.H. and A.P.; investigation, M.S., I.B., L.H., J.B., C.A., V.G., L.B. and R.A.H.; writing of original draft, M.S., I.B., L.H., R.A.H. and A.P.; writing, review and editing, M.S., I.B., R.A.H. and A.P.; visualization, M.S. and I.B.; supervision, A.P.; project administration, A.P.; and funding acquisition, A.P.

Funding

This work was supported by the Centre Nationnal de la Recherche Scientifique (University Paris 7) and the Fondation ARC pour la recherche sur le Cancer (155032). I.B. was supported by the ARC and by the Ligue Contre le Cancer; L.H. was supported by Université Paris Diderot and the Fondation ARC pour la recherche sur le Cancer; C.A. was supported by the Association Franco-argentine and by the Fondation ARC pour la recherche sur le Cancer; L.B. was supported by Paris Sorbonne Cité.

Supplementary information

Supplementary information available online at
http://dev.biologists.org/lookup/doi/10.1242/dev.144782.supplemental

References

Alves, G., Limbourg-Bouchon, B., Tricoire, H., Brissard, Z. J., Lamour, I. C. and Busson, D. (1998). Modulation of Hedgehog target gene expression by the Fused serine- threonine kinase in wing imaginal discs. *Mech. Dev.* **78**, 17-31.

Ayers, K. L. and Thérond, P. P. (2010). Evaluating Smoothened as a G-protein-coupled receptor for Hedgehog signalling. *Trends Cell Biol.* **20**, 287-298.

Aza, B. P. and Kornberg, T. B. (1999). Ci: a complex transducer of the hedgehog signal. *Trends Genet.* **15**, 458-462.

Chen, Y. and Jiang, J. (2013). Decoding the phosphorylation code in Hedgehog signal transduction. *Cell Res.* **23**, 186-200.

Chen, W., Ren, X. R., Nelson, C. D., Barak, L. S., Chen, J. K., Beachy, P. A., de Sauvage, F. and Lefkowitz, R. J. (2004). Activity-dependent internalization of smoothened mediated by beta-arrestin 2 and GRK2. *Science* **306**, 2257-2260.

Claret, S., Sanial, M. and Plessis, A. (2007). Evidence for a novel feedback loop in the Hedgehog pathway involving Smoothened and Fused. *Curr. Biol.* **17**, 1326-1333.

Crozatier, M., Glise, B., Khemici, V. and Vincent, A. (2003). Vein-positioning in the Drosophila wing in response to Hh: new roles of Notch signaling. *Mech. Dev.* **120**, 529-535.

Fan, J., Liu, Y. and Jia, J. (2012). Hh-induced Smoothened conformational switch is mediated by differential phosphorylation at its C-terminal tail in a dose- and position-dependent manner. *Dev. Biol.* **366**, 172-184.
Fan, J., Jiang, K., Liu, Y. and Jia, J. (2013). Hrs promotes ubiquitination and mediates endosomal trafficking of smoothened in Drosophila hedgehog signaling. *PLoS ONE* **8**, e79021.
Ferrell, J. E., Jr and Ha, S. H. (2014a). Ultrasensitivity part II: multisite phosphorylation, stoichiometric inhibitors, and positive feedback. *Trends Biochem. Sci.* **39**, 556-569.
Ferrell, J. E., Jr and Ha, S. H. (2014b). Ultrasensitivity part III: cascades, bistable switches, and oscillators. *Trends Biochem. Sci.* **39**, 612-618.
Guerrero, I. and Kornberg, T. B. (2014). Hedgehog and its circuitous journey from producing to target cells. *Semin. Cell Dev. Biol.* **33**, 52-62.
Ho, K. S., Suyama, K., Fish, M. and Scott, M. P. (2005). Differential regulation of Hedgehog target gene transcription by Costal2 and Suppressor of Fused. *Development* **132**, 1401-1412.
Ingham, P. W., Nakano, Y. and Seger, C. (2011). Mechanisms and functions of Hedgehog signalling across the metazoa. *Nat. Rev. Genet.* **12**, 393-406.
Jia, J., Tong, C. and Jiang, J. (2003). Smoothened transduces Hedgehog signal by physically interacting with Costal2/Fused complex through its C-terminal tail. *Genes Dev.* **17**, 2709-2720.
Jia, J., Tong, C., Wang, B., Luo, L. and Jiang, J. (2004). Hedgehog signalling activity of Smoothened requires phosphorylation by protein kinase A and casein kinase I. *Nature* **432**, 1045-1050.
Jia, H., Liu, Y., Xia, R., Tong, C., Yue, T., Jiang, J. and Jia, J. (2010). Casein kinase 2 promotes Hedgehog signaling by regulating both smoothened and Cubitus interruptus. *J. Biol. Chem.* **285**, 37218-37226.
Jiang, K., Liu, Y., Fan, J., Epperly, G., Gao, T., Jiang, J. and Jia, J. (2014). Hedgehog-regulated atypical PKC promotes phosphorylation and activation of Smoothened and Cubitus interruptus in Drosophila. *Proc. Natl. Acad. Sci. USA* **111**, E4842-E4850.
Kupinski, A. P., Raabe, I., Michel, M., Ail, D., Brusch, L., Weidemann, T. and Bokel, C. (2013). Phosphorylation of the Smo tail is controlled by membrane localisation and is dispensable for clustering. *J. Cell Sci.* **126**, 4684-4697.
Lander, A. D. (2007). Morpheus unbound: reimagining the morphogen gradient. *Cell* **128**, 245-256.
Lee, R. T., Zhao, Z. and Ingham, P. W. (2016). Hedgehog signalling. *Development* **143**, 367-372.
Li, S., Chen, Y., Shi, Q., Yue, T., Wang, B. and Jiang, J. (2012). Hedgehog-regulated ubiquitination controls smoothened trafficking and cell surface expression in Drosophila. *PLoS Biol.* **10**, e1001239.
Li, S., Li, S., Han, Y., Tong, C., Wang, B., Chen, Y. and Jiang, J. (2016). Regulation of smoothened phosphorylation and high-level hedgehog signaling activity by a plasma membrane associated kinase. *PLoS Biol.* **14**, e1002481.
Liu, Y., Cao, X., Jiang, J. and Jia, J. (2007). Fused-Costal2 protein complex regulates Hedgehog-induced Smo phosphorylation and cell-surface accumulation. *Genes Dev.* **21**, 1949-1963.
Lum, L., Zhang, C., Oh, S., Mann, R. K., von Kessler, D. P., Taipale, J., Weis-Garcia, F., Gong, R., Wang, B. and Beachy, P. A. (2003). Hedgehog signal transduction via Smoothened association with a cytoplasmic complex scaffolded by the atypical kinesin, Costal-2. *Mol. Cell* **12**, 1261-1274.
Maier, D., Cheng, S. and Hipfner, D. R. (2012). The complexities of G-protein-coupled receptor kinase function in Hedgehog signaling. *Fly (Austin)* **6**, 135-141.
Maier, D., Cheng, S., Faubert, D. and Hipfner, D. R. (2014). A broadly conserved g-protein-coupled receptor kinase phosphorylation mechanism controls Drosophila smoothened activity. *PLoS Genet.* **10**, e1004399.
Malpel, S., Claret, S., Sanial, M., Brigui, A., Piolot, T., Daviet, L., Martin-Lannerée, S. and Plessis, A. (2007). The last 59 amino acids of Smoothened cytoplasmic tail directly bind the protein kinase Fused and negatively regulate the Hedgehog pathway. *Dev. Biol.* **303**, 121-133.
Martin, V., Carrillo, G., Torroja, C. and Guerrero, I. (2001). The sterol-sensing domain of Patched protein seems to control Smoothened activity through Patched vesicular trafficking. *Curr. Biol.* **11**, 601-607.
Monnier, V., Dussillol, F., Alves, G., Lamour-Isnard, C. and Plessis, A. (1998). Suppressor of fused links fused and Cubitus interruptus on the hedgehog signalling pathway. *Curr. Biol.* **8**, 583-586.
Monnier, V., Ho, K. S., Sanial, M., Scott, M. P. and Plessis, A. (2002). Hedgehog signal transduction proteins: contacts of the Fused kinase and Ci transcription factor with the kinesin-related protein Costal2. *BMC Dev. Biol.* **2**, 4.
Motzny, C. K. and Holmgren, R. (1995). The Drosophila cubitus interruptus protein and its role in the wingless and hedgehog signal transduction pathways. *Mech. Dev.* **52**, 137-150.
Nakano, Y., Guerrero, I., Hidalgo, A., Taylor, A., Whittle, J. R. S. and Ingham, P. W. (1989). A protein with several possible membrane-spanning domains encoded by the *Drosophila* segment polarity gene *patched*. *Nature* **341**, 508-513.
Ogden, S. K., Ascano, M., Jr, Stegman, M. A., Suber, L. M., Hooper, J. E. and Robbins, D. J. (2003). Identification of a functional interaction between the transmembrane protein Smoothened and the kinesin-related protein Costal2. *Curr. Biol.* **13**, 1998-2003.
Ohlmeyer, J. T. and Kalderon, D. (1998). Hedgehog stimulates maturation of Cubitus interruptus into a labile transcriptional activator. *Nature* **396**, 749-753.
Pak, E. and Segal, R. A. (2016). Hedgehog signal transduction: key players, oncogenic drivers, and cancer therapy. *Dev. Cell* **38**, 333-344.
Ranieri, N., Therond, P. P. and Ruel, L. (2014). Switch of PKA substrates from Cubitus interruptus to Smoothened in the Hedgehog signalosome complex. *Nat. Commun.* **5**, 5034.
Ruel, L., Gallet, A., Raisin, S., Truchi, A., Staccini-Lavenant, L., Cervantes, A. and Therond, P. P. (2007). Phosphorylation of the atypical kinesin Costal2 by the kinase Fused induces the partial disassembly of the Smoothened-Fused-Costal2-Cubitus interruptus complex in Hedgehog signalling. *Development* **134**, 3677-3689.
Shi, Q., Li, S., Jia, J. and Jiang, J. (2011). The Hedgehog-induced Smoothened conformational switch assembles a signaling complex that activates Fused by promoting its dimerization and phosphorylation. *Development* **138**, 4219-4231.
Su, Y., Ospina, J. K., Zhang, J., Michelson, A. P., Schoen, A. M. and Zhu, A. J. (2011). Sequential phosphorylation of smoothened transduces graded hedgehog signaling. *Sci. Signal.* **4**, ra43.
Tirat, A., Freuler, F., Stettler, T., Mayr, L. M. and Leder, L. (2006). Evaluation of two novel tag-based labelling technologies for site-specific modification of proteins. *Int. J. Biol. Macromol.* **39**, 66-76.
Vervoort, M. (2000). hedgehog and wing development in Drosophila: a morphogen at work? *BioEssays* **22**, 460-468.
Wang, Q. T. and Holmgren, R. A. (2000). Nuclear import of cubitus interruptus is regulated by hedgehog via a mechanism distinct from Ci stabilization and Ci activation. *Development* **127**, 3131-3139.
Xia, R., Jia, H., Fan, J., Liu, Y. and Jia, J. (2012). USP8 promotes smoothened signaling by preventing its ubiquitination and changing its subcellular localization. *PLoS Biol.* **10**, e1001238.
Zadorozny, E. V., Little, J. C. and Kalderon, D. (2015). Contributions of Costal 2-Fused interactions to Hedgehog signaling in Drosophila. *Development* **142**, 931-942.
Zhao, Y., Tong, C. and Jiang, J. (2007). Hedgehog regulates smoothened activity by inducing a conformational switch. *Nature* **450**, 252-258.
Zhao, Z., Lee, R. T. H., Pusapati, G. V., Iyu, A., Rohatgi, R. and Ingham, P. W. (2016). An essential role for Grk2 in Hedgehog signalling downstream of Smoothened. *EMBO Rep.* **17**, 739-752.
Zhou, Q. and Kalderon, D. (2010). Costal 2 interactions with Cubitus interruptus (Ci) underlying Hedgehog-regulated Ci processing. *Dev. Biol.* **348**, 47-57.
Zhou, Q. and Kalderon, D. (2011). Hedgehog activates fused through phosphorylation to elicit a full spectrum of pathway responses. *Dev. Cell* **20**, 802-814.
Zhu, A. J., Zheng, L., Suyama, K. and Scott, M. P. (2003). Altered localization of Drosophila Smoothened protein activates Hedgehog signal transduction. *Genes Dev.* **17**, 1240-1252.

Supplemental Information

Supplemental Figure Legends Figures S1-S8

Figure S1. Activated FU promotes the phosphorylation of the four Ct clusters.

(A) Immunodetection of SMO-HA in extracts of Cl8 cells transiently expressing SMO^{wt}-HA, SMO $^{PKA-SA}$-HA and SMO $^{PKA-SD}$-HA with GAP-GFP-FU. Samples in lanes 3, 6 and 9 were treated with phosphatase inhibitor (Phos Inhibitor) and samples in lanes 2, 5 and 8 were treated with λ-phosphatase (λ-phos). These results indicate that the shift in the migration of SMO^{wt}, SMO^{PKA-SA} and SMO^{PKA-SD} in presence of GAP-CFP-FU is due to phosphorylation. In all the panels, the black arrow and the bracket indicate the non-phosphorylated (SMO) and the phosphorylated (p-SMO) forms of SMO respectively.

(B) Immunodetection of SMO-HA in extracts of Cl8 cells transiently expressing SMO^{wt}-HA (lanes 1-2), SMO^{Ct-SA}-HA (lane 3), SMO^{GI-SA}-HA (lane 4), SMO^{GII-SA}-HA (lane 5), SMO$^{GIII-SA}$-HA (lane 6) and SMO^{GIV-SA}-HA (lane 7) without ("-") or with ("+") GAP-MYC-FU. Mutation of the S in group II suppressed most of the phosphorylation of SMO^{GII-SA}. For SMO^{GIV-SA} the shift of p-SMO was little affected but there was a reproducible modest decrease of pSMO/SMO. Finally, mutation of group I and III had intermediate effects.

(C) SMO^{wt}-HA (lanes 1, 2), SMO^{Δ978} –HA (lanes 3, 4) without ("-") or with ("+") GAP-GFP-FU. This indicates that GAP-GFP-FU has little effect on the phosphorylation of SMO^{Δ978} (a form of SMO which lacks its FU binding region.

(D) Immunodetection of SMO-HA in extracts of Cl8 cells transiently expressing SMO^{wt}-HA, SMO^{wt}-HA + HH, SMO^{Ct-SD} -HA, SMO$^{PKA-SA\ Ct-SD}$-HA. Samples in lanes 3, 6 and 9 were treated with phosphatase inhibitor (Phos Inhibitor) and samples in lanes 4, 7 and 10 were treated with λ-phosphatase (λ-phos). These results indicate that the shift of SMO^{Ct-SD} in absence of HH is probably not due to phosphorylation.

(E) Immunodetection of forms of SMO-HA in extracts of Cl8 cells transiently expressing SMO^{Ct-SD}-HA (lanes 1-2) and SMO$^{PKA-SA\ Ct-SD}$-HA (lanes 3-4) without ("-") or with ("+") HH. This indicates that SMO^{Ct-SD} is still phosphorylated in presence of HH.

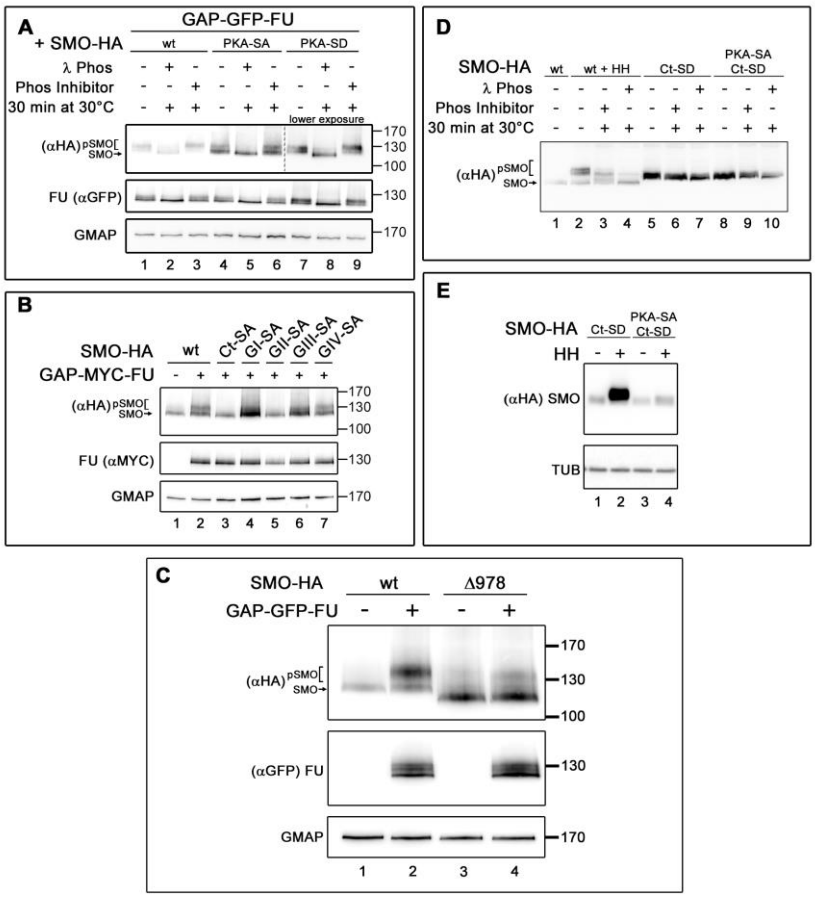

Figure S2. The SNAP-SMO fusion is functional *in vivo*.

Wings of *UAS dicer; nub> RNAi smo5'UTR* **(A)**, *UAS dicer; nub> RNAi smo5'UTR; UAS smo* **(B)**, or *UAS dicer; nub> RNAi smo5'UTR; UAS snap-smo* flies **(C)**. Male with a reduced *smo* expression presented a loss of LV3 and LV4 and a decrease in the size of the wing due to a strong downregulation of HH pathway. Overexpression of *smo* or *snap-smo* similarly suppressed these effects restoring both the formation of LV3 and LV4 and the normal size of the wing, leading of a normal phenotype.

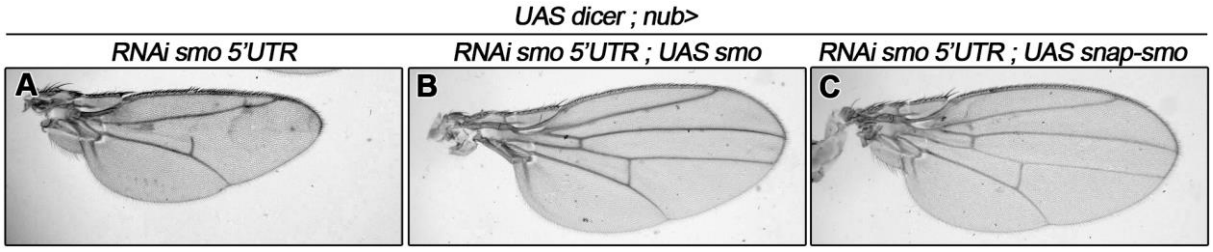

Figure S3. Phosphorylation of the Ct-sites controls SMO accumulation at the plasma membrane.

(A) Cell surface fraction of SMO (normalized to GLIP-GUS) expressed as a ratio to the amount of SMO^{wt} for the different SNAP-SMO constructs. Light Green is without HH and dark green with HH.

(B) Amount of the intracellular SMO (normalized to GLIP-GUS) and expressed as a ratio to the amount of SMO^{wt} for the different SNAP-SMO constructs. Pink is without HH and red with HH.

(C) Confocal images of Cl8 cells transiently transfected with various forms of SNAP-SMO-RFP with or without HH. Cells were washed in PBS 48h after transfection and labeled for 10 minutes in complete cell medium with 0.75µM SNAP Surface 488nm (green). Then cells were quickly washed in PBS and fixed in PFA 4% for ten minutes. Images of cells were acquired with a confocal spinning disc CSU10 (Yokawaga) analysed with ImageJ software (National Institute of Health), and assembled with Photoshop (Adobe, San Jose, CA). This confirms the localization of the various forms of SMO.

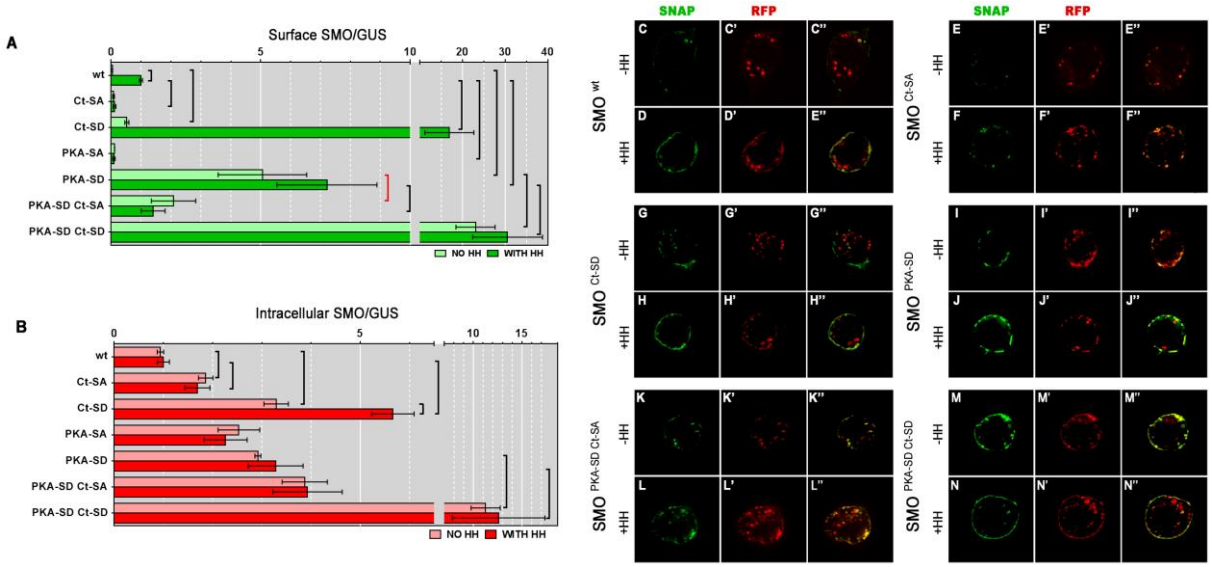

Figure S4: Phosphorylation of the Ct-sites controls SMO level and localization *in vivo*.

(A-C) XY confocal images of wing disc expressing *UAS snap-smo^{wt}* (A), *UAS snap-smo$^{Ct\text{-}SA}$* (B) and *UAS snap-smo$^{Ct\text{-}SD}$* (C) driven by *apGAL4* and labeled with a non-liposoluble fluorescent substrate. The imaging conditions used are exactly the same for each genotype. These data confirm *in vivo* that the phosphorylation by FU increase SMO level.

(D-F) XY confocal images of wing disc expressing *UAS smo^{wt}* (D), *UAS smo$^{Ct\text{-}SA}$* (E) and *UAS smo$^{Ct\text{-}SD}$* (F) driven by *MS1096* and stained with an antibody against SMO. The square in (D1,E1,F1) corresponds to the region enlarged in (D2,E2,F2).

The white broken lines delimit the A/P border.

Here and in the following figures, XY disc images are oriented dorsal up and anterior left.

(G-I) Single XZ confocal section perpendicular to the A/P axis through the dorsal compartment of wing discs of *apGAL4* flies expressing *UAS smo^{wt}* (G), *UAS smo$^{Ct\text{-}SA}$* (H) and *UAS smo$^{Ct\text{-}SD}$* (I) and stained with antibodies against SMO (white in G1-I1 or red in G2-I2), aPKC (G2-I2, green) and CI-FL (G2-I2, blue). The 2 arrowheads indicate the A/P boundary. Ap for apical; Ba for basal. Note that different imaging conditions were used to optimize the acquisition of SMO for each genotype.

Scale bars represent 50 µm in (A, B, C, D1, E1, F1) and 20 µm in the enlargement (D2, E2, F2, G, H, I).

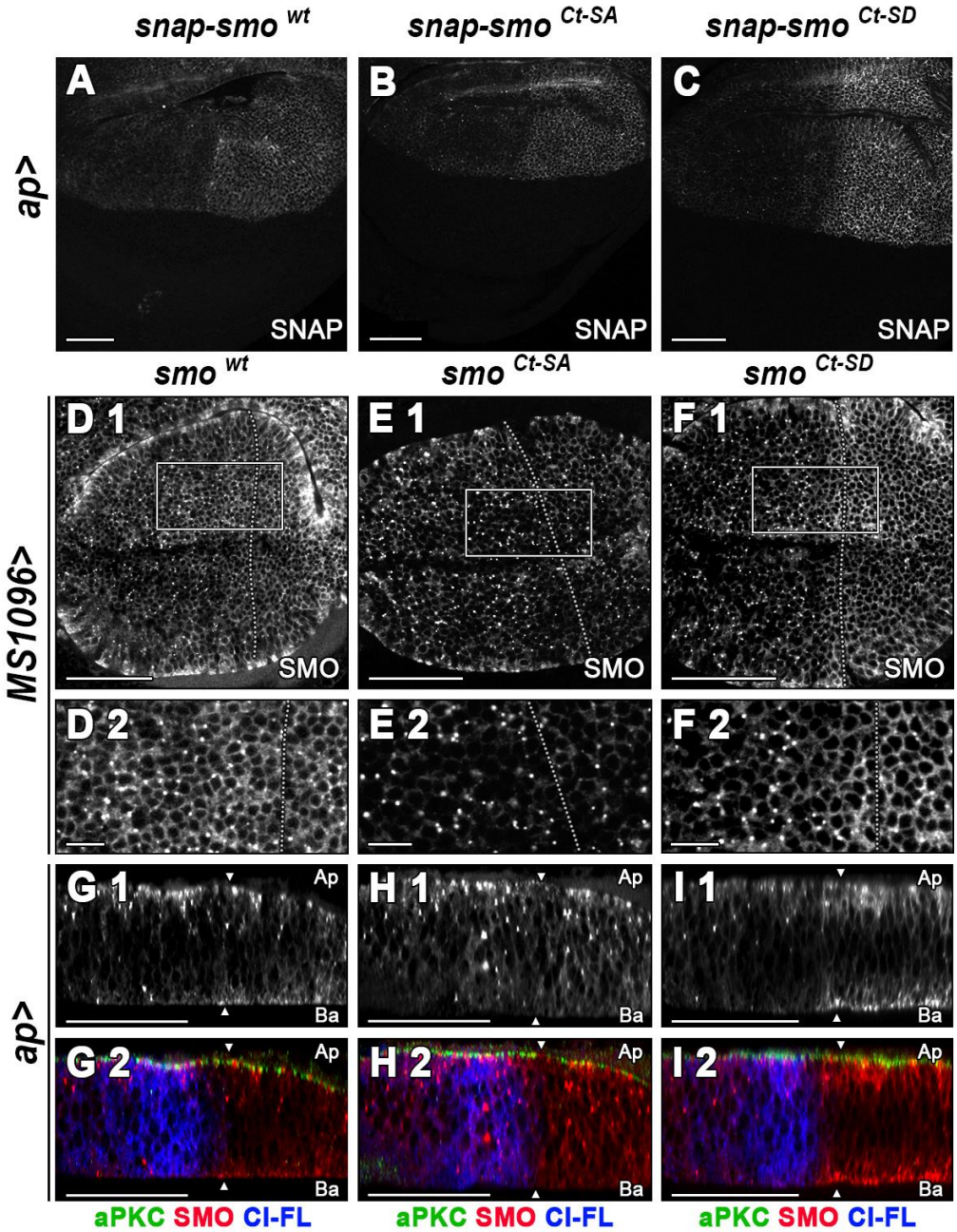

Figure S5. Phosphorylation of the Ct-sites increases the effects of PKA/CKI phosphorylation.

Wing discs of *apGAL4* flies expressing *UAS smo*^{wt} (A), *UAS smo*$^{PKA\text{-}SD}$ (B), *UAS smo*$^{PKA\text{-}SD\ Ct\text{-}SD}$ (C) and *UAS smo*$^{PKA\text{-}SD\ Ct\text{-}SA}$ (D) and stained with antibodies against PTC (A1-D1) and *β–galactosidase* to follow *iro-Z* transcriptional fusion reporters (A2-D2). Scale bar represent 50μm. These data confirm the ones observed with *ptc-Z* and *dpp-Z* staining (Fig. 4).

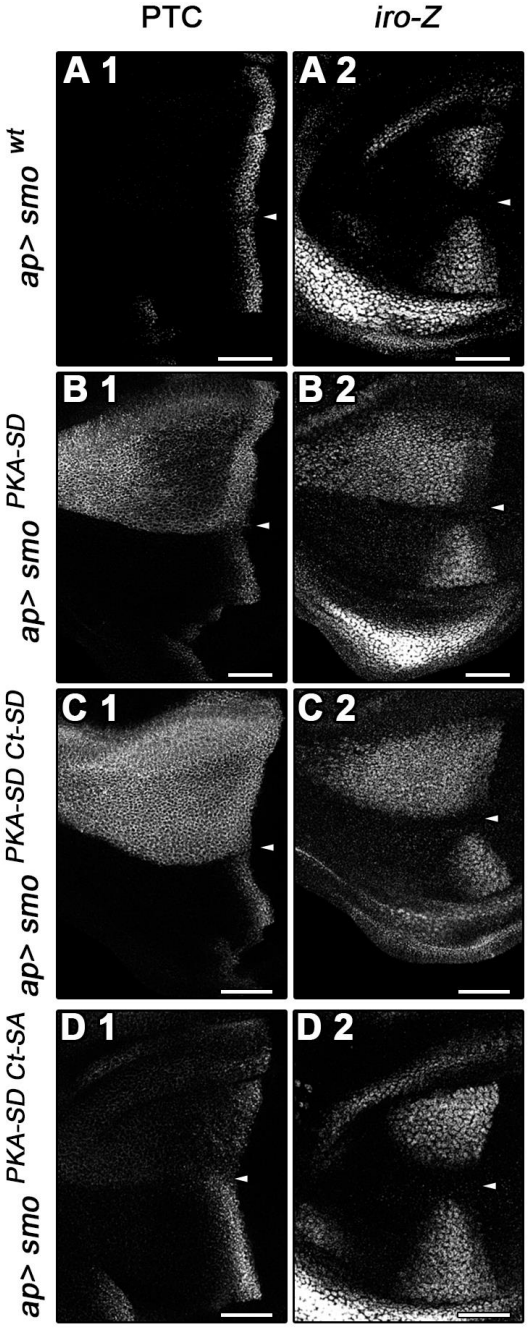

Figure S6: SMO$^{PKA\text{-}SD\ Ct\text{-}SA}$ has also a negative effect in absence of endogenous smoothened

Wing discs flies with *smo* mutant MARCM clones vizualised by GFP and expressing *UAS smo^{wt}* (A, C) or *UAS smo$^{PKA\text{-}SD\ Ct\text{-}SA}$* (B, D) and stained with antibodies against CI and COL or PTC as indicated. The clones are outlined with dotted line. These data confirm with the effects observed in a wild type *smo* background (Fig. 4).
Scale bar represent 50µm.

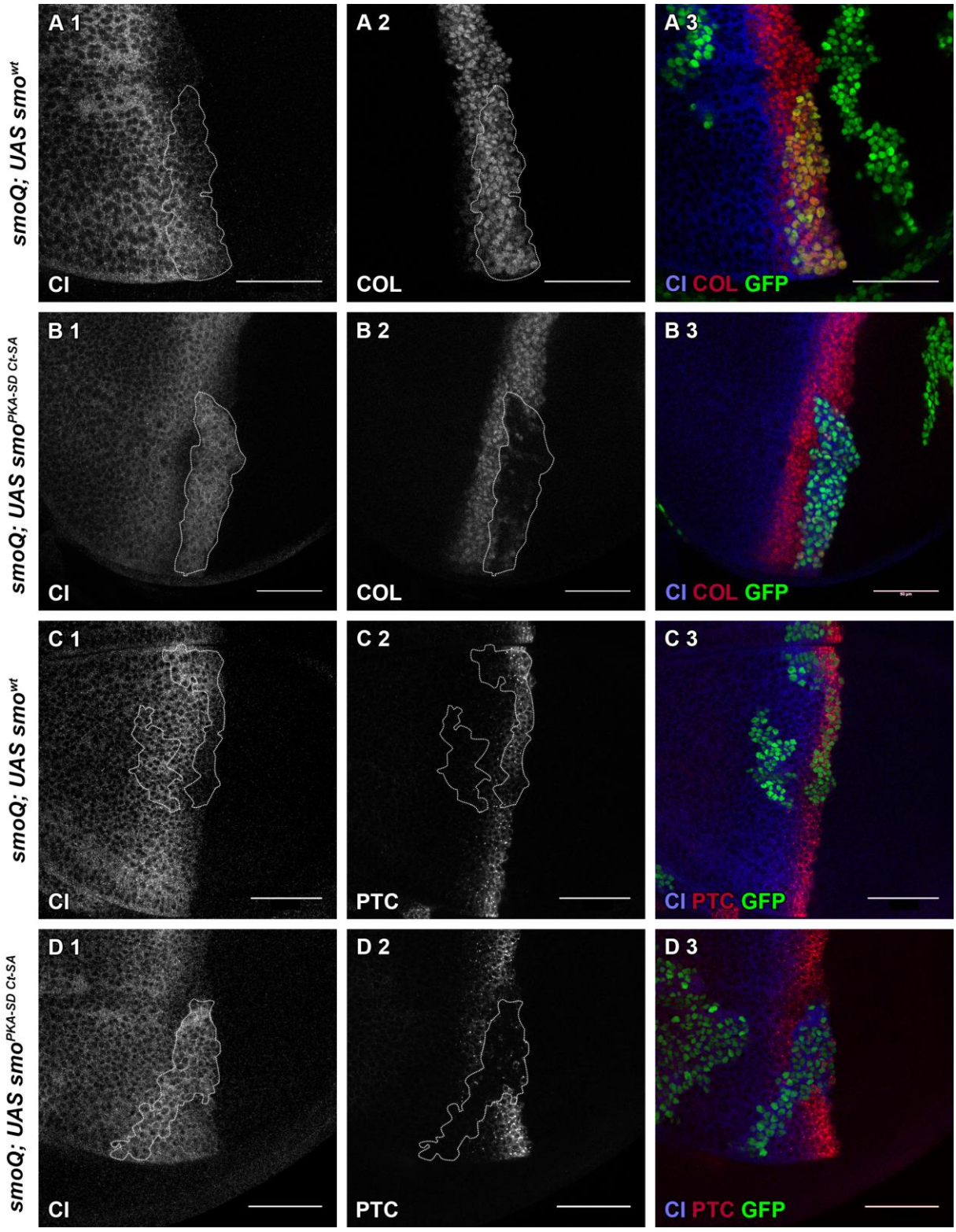

Figure S7. The negative effects of SMO$^{PKA\text{-}SD\ Ct\text{-}SA}$ is suppressed by coexpression of constitutively active FU.
Wing discs of *apGAL4* flies alone (A) or expressing *UAS smo$^{PKA\text{-}SD\ Ct\text{-}SA}$* (B), *UAS GAP-cFU* (C) and *UAS GAP-cFU* with *UAS-smo$^{PKA\text{-}SD\ Ct\text{-}SA}$* (D) and stained with antibodies against PTC (A1-D1) and *β–galactosidase* to follow *dpp-Z* (A2-D2). These data confirm the ones observed with *ptc-Z* and *iro-Z* staining (Fig. 5).
Scale bar represent 50μm.

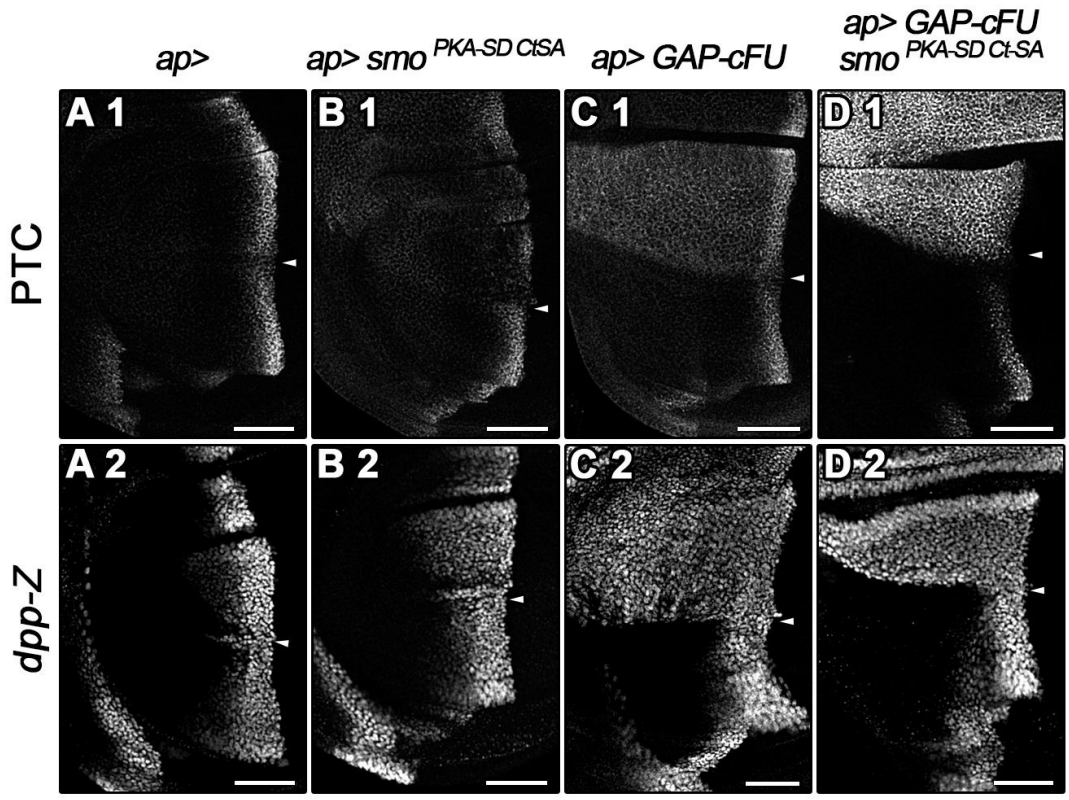

Figure S8: The effects of GAP-cFU overexpression are enhanced in the presence of SMO$^{PKA\text{-}SD}$
Wing discs of *apGAL4* flies expressing *UAS smo$^{PKA\text{-}SD}$* (A), *UAS GAP-cFU* (B) and *UAS GAP-cFU* with *UAS smo$^{PKA\text{-}SD}$* (C) and stained with antibodies against PTC. Expression of GAP-cFU and SMO$^{PKA\text{-}SD}$ led to anterior expansion of the expression of PTC. Note that the effects are stronger when GAP-cFU and SMO$^{PKA\text{-}SD}$ are expressed together.

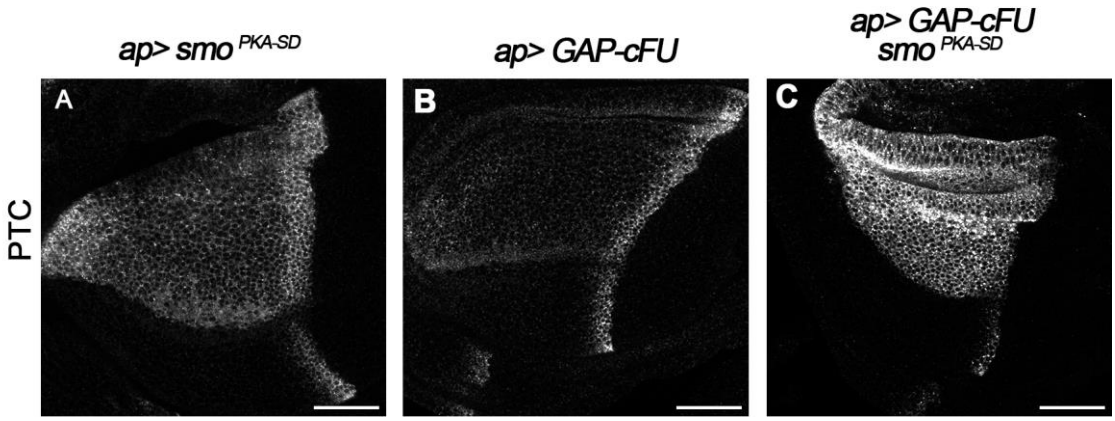

Supplemental Experimental procedures

Drosophila strains and genetics

The following constructs and transgenic lines were previously published: *ap-gal4* (Chr II, (Weihe et al., 2001)), *MS1096* (chr. X (Capdevila et al., 1994)), *dppZ* (Twombly et al., 1996), *ptcZ* (Struhl et al., 1997), *iroZ* (Dambly-Chaudiere and Leyns, 1992). The *UAS-smo*, *UAS-smo*$^{Ct\text{-}SD/SA}$, *UAS-smo*$^{GI\ to\ IV\ SA}$, *UAS-smo*$^{PKA\text{-}SD/SA}$, *UAS-smo*$^{PKA\text{-}SD/SA,Ct\text{-}SD/SA}$, *UAS-snap-smo*$^{wt/Ct\text{-}SD/Ct\text{-}SA}$ transgenic flies were generated in this work by BestGene Inc. All *smo* transgenes were introduced into the same landing site (9738) on 3R (at 99F8) using the *PhiC31* integration system to ensure that they are expressed at similar levels (Bateman et al., 2006). The following drosophila genotypes were used to generate MARCM clones: (1) *hs-FLP122, tubG4, UAS/GFP/FM7; FRT40A, tub GAL80* (2) *FRT40A smo*^{Q}*/CyO; UAS-smo*^{WT} and (3) *FRT40A smo*^{Q}*/CyO; UAS-smo*$^{PKA\text{-}SD,\ Ct\text{-}SA}$. Heat-shock was induced 3, 4 days after egg laying for 2 hours at 37°. Fly wings were dissected in 70% ethanol and mounted in Hoyer's medium. Pictures were taken with a Zeiss Lumar stereomicroscope and the AxioVision software. For the functional assays, the flies were grown at 29°C unless indicated otherwise.

Imaginal discs immunostaining

Imaginal discs from third-instar wandering larvae were dissected in phosphate buffered saline (PBS), fixed by incubation for 20 min at room temperature (RT) in 4% paraformaldehyde, washed, and permeabilized by 3 incubations for 10 min each in PBS + 0.3% triton (PBST). They were blocked by incubation for 1 hr in PBST+ BSA 0.1% + NaCL 0.25M and then overnight at 4°c with the primary antibody. They were washed four times for 10 min with PBST+ BSA 0.1% + NaCL 0.25M and incubated for 2 hr at RT with the secondary antibody (in PBST+ BSA 0.1% + NaCL 0.25M). Finally they were rinsed 3 times for 10 min each in PBST and mounted in All the images of wing imaginal discs (at least twenty discs per genotype) were acquired with a Leica SP5 confocal microscope, analyzed with ImageJ software (National Institute of Health), and assembled with Photoshop (Adobe, San Jose, CA). The primary antibodies used were the following: mouse anti-PTC, 1:1000 (Apa 1, from Developmental Studies Hybridoma Bank [DHSB]) (Martin et al., 2001), mouse anti-SMO, 1:100 (20C6, from DSHB) (Lum et al., 2003), mouse anti-COL, 1:100 (Gift from M. Crozatier) (Crozatier et al., 2003), rat anti-full length CI, 1:5 (2A1 from R. Holmgren (Motzny and Holmgren, 1995)), and rabbit polyclonal anti-β-galactosidase 1/100 (ABR-Affinity BioReagents). Secondary antibodies were obtained from Molecular probe and were all used at a dilution of 1:100.

Plasmids

We used the Gateway Technology (Invitrogen following the manufacturer's instructions) to introduce the wild-type and mutant *smo* transgenes in the vectors *pAct5C-GW-HA* (gifts from T. Murphy) that allowed the expression of the SMO (tagged with a triple HA on its C-terminus under an actin5C promoter) for tissue culture cell transfection and *pUASt-GW-attB* (constructed by A. Brigui by insertion of the GW recombination cassette C3 at the EcoRI site of the *pUASt-attB* plasmid (GI EF362409)) for PhiC31 germline transformation, respectively. Prior to that, the PCR products obtained from the coding sequence (without the termination codon) of a *smo*^{wt} cDNA were inserted into *pENTR/D-TOPO* by directional TOPO Cloning. Mutations leading to the S to A and S to D changes of the PKA/CKI sites were inserted into *pENTR/D-TOPO-smo* by replacement of a region by the similar region coming from *smo*$^{PKA\text{-}SD/SA}$ from (Jia et al., 2004), leading to *pENTR/D-TOPO-smo*$^{PKA\text{-}SA}$ and *pENTR/D-TOPO-smo*$^{PKA\text{-}SD}$. The mutations leading to the S to A and S to D replacements of the clusters I to IV were introduced into *pENTR/D-TOPO-smo* by site-directed mutagenesis (QuickChange Kit, Stratagene), leading to the *pENTR/D-TOPO smo*$^{CtGI\ to\ IV\text{-}SA}$ and *pENTR/D-TOPO smo* $^{CtGI\ to\ IV\text{-}SD}$. *pENTR/D-TOPO smo*$^{Ct\text{-}SA}$, *pENTR/D-TOPO smo*$^{Ct\text{-}SD}$ and the *pENTR/D-TOPO* carrying the various combination of PKA-SA/SD and FU-SA/SD mutations were made by assembling PCR fragments from the corresponding mutant *smo* cDNA constructs. All constructs were checked by sequencing the fragments produced by PCR and their junctions

Cl8 cell culture, transfection and Western Blotting

Cl8 cells were cultured as described in (Claret et al., 2007) in 2% CFS (Hyclone). Transient transfections were then carried out with Transit Insect Reagent (Mirus). 48h post transfection, cells were harvested and washed twice in PBS1X, lysed in 1% NP-40, 150 mM NaCl, 50 mM Tris pH 8, 0.5% sodium deoxycholate, 10% glycerol with "Complete EDTA free antiprotease mix" (Roche) and "Phosphatase Inhibitor Cocktail Set II" (Calbiochem) and passed 3 times in a 26g needle. The lysate was centrifuged (12000 rcf) 10 minutes at 4°C, and mix with Laemmli sample buffer (Bio-Rad) and 0.1M DTT. Protein concentrations were assayed by the Bradford method, using the Bradford Ultra reagent (Expedeon) according to the manufacturer instructions. The equivalent of 60µg of protein was warmed 5 minutes at 25°C before loading on a 10% Anderson gel. The gels were run using a miniprotean apparatus (Bio-Rad) 90 minutes at 150 volts (constant voltage). The proteins were then transferred for 75 minutes at 100V onto Nitrocellulose membrane (0,2µM, Protran BA 83 Schleicher & Schuell) using the same apparatus

and blotted with 1:1000 Rat monoclonal anti-HA (Roche), 1:5000 Rabbit anti-GFP (Torrey Pines Biolabs), 1:2000 Rabbit anti-GMAP (Sigma, gift from Laurent Ruel), 1:1000 Mouse anti-Myc (clone 4A6, Millipore), secondary antibodies conjugated with HRP: anti-Rat (JacksonImmuno), anti-Mouse (Sigma) and anti-Rabbit (JacksonImmuno). The immunolabeled bands were detected with the enhanced chemiluminescence detection system (ECL Select, Amersham) on a LAS-3000 imager (Fujifilm). For wing disc blot, discs were dissected in PBS and transferred in lysis NP40 buffer mix with Laemmli sample buffer 0.1M DTT, passed 3 times in a 26g needle and frozen in liquid nitrogen. Samples were run as for CL8 extracts. Membrane was blotted using 1:1000 Rabbit anti-SMO (gift from P. Thérond) and 1:1000 Mouse anti α-tub (Sigma).

Bateman, J. R., Lee, A. M. and Wu, C. T. (2006). Site-specific transformation of Drosophila via phiC31 integrase-mediated cassette exchange. *Genetics* **173**, 769-777.

Capdevila, J., Pariente, F., Sampedro, J., Alonso, J. L. and Guerrero, I. (1994). Subcellular localization of the segment polarity protein patched suggests an interaction with the wingless reception complex in Drosophila embryos. *Development* **120**, 987-998.

Claret, S., Sanial, M. and Plessis, A. (2007). Evidence for a novel feedback loop in the Hedgehog pathway involving Smoothened and Fused. *Curr Biol* **17**, 1326-1333.

Crozatier, M., Glise, B., Khemici, V. and Vincent, A. (2003). Vein-positioning in the Drosophila wing in response to Hh; new roles of Notch signaling. *Mech Dev* **120**, 529-535.

Dambly-Chaudiere, C. and Leyns, L. (1992). The determination of sense organs in Drosophila: a search for interacting genes. *Int J Dev Biol* **36**, 85-91.

Jia, J., Tong, C., Wang, B., Luo, L. and Jiang, J. (2004). Hedgehog signalling activity of Smoothened requires phosphorylation by protein kinase A and casein kinase I. *Nature* **432**, 1045-1050.

Lum, L., Zhang, C., Oh, S., Mann, R. K., von Kessler, D. P., Taipale, J., Weis-Garcia, F., Gong, R., Wang, B. and Beachy, P. A. (2003). Hedgehog signal transduction via Smoothened association with a cytoplasmic complex scaffolded by the atypical kinesin, Costal-2. *Mol Cell* **12**, 1261-1274.

Martin, V., Carrillo, G., Torroja, C. and Guerrero, I. (2001). The sterol-sensing domain of Patched protein seems to control Smoothened activity through Patched vesicular trafficking. *Curr Biol* **11**, 601-607.

Motzny, C. K. and Holmgren, R. (1995). The Drosophila cubitus interruptus protein and its role in the wingless and hedgehog signal transduction pathways. *Mech. Dev.* **52**, 137-150.

Struhl, G., Barbash, D. A. and Lawrence, P. A. (1997). Hedgehog organises the pattern and polarity of epidermal cells in the Drosophila abdomen. *Development* **124**, 2143-2154.

Twombly, V., Blackman, R. K., Jin, H., Graff, J. M., Padgett, R. W. and Gelbart, W. M. (1996). The TGF-beta signaling pathway is essential for Drosophila oogenesis. *Development* **122**, 1555-1565.

Weihe, U., Milan, M. and Cohen, S. M. (2001). Regulation of Apterous activity in Drosophila wing development. *Development* **128**, 4615-4622.